CERN-ACC-2018-0045
17 March 2019

Higgs and Electro-weak symmetry breaking at the FCC-hh

L. Borgonovi[*], S. Braibant[*], B. Di Micco[†], E. Fontanesi[*], P. Harris[‡], C. Helsens[§], D. Jamin[§], M.L. Mangano[§], G. Ortona[¶], M. Selvaggi[1)§], A. Sznajder[‖], M. Testa[¶], M. Verducci[¶]

On behalf of the FCC-hh Collaboration

[*] *Università di Bologna, Italy,*
[†] *Università degli Studi Roma Tre, Italy,*
[‡] *Massachusetts Institute of Technology (MIT), Cambridge, USA,*
[§] *European Organization for Nuclear Research (CERN), Geneva, Switzerland,*
[¶] *Laboratoire Leprince-Ringuet, Ecole Polytechnique (LLR), Palaiseau, France,*
[‖] *Universidade do Estado do Rio de Janeiro (UERJ), Rio de Janeiro, Brazil*

Abstract

The future circular hadron-hadron collider FCC-hh is expected to produce collisions at the center of mass energy of $\sqrt{s} = 100$ TeV and to deliver an integrated luminosity of $30\,\text{ab}^{-1}$. The Higgs-self coupling will be measured with a 5% precision via double Higgs production. Tens of billions of Higgs bosons will be produced at the FCC-hh. Such large statistics will allow for a wide range of possibilities in the realm of precision Higgs measurements. Several Higgs couplings will be measured to a percent level precision, including the second generation muon yukawa coupling. The Higgs to invisible branching fraction will be probed to a level of few 10^{-4} and the rate of longitudinally polarized vector bosons produced in vector boson scattering will be measured with 2% precision.

[1] michele.selvaggi@cern.ch

Contents

1 Introduction

With the discovery [1, 2] of the Higgs particle [3–8] at the LHC the Standard Model is now complete. The scalar sector of the SM is however the less understood part of the theory. The principles dictating its structure are still unclear. Not surprisingly, many of the open problems of the SM are connected to the Higgs sector. For example, the stability of the Higgs mass [9] and of the Electroweak (EW) scale in general against UV-sensitive radiative corrections motivate the existence of new symmetries near the TeV scale. To address these questions, possible theoretical extensions of the SM have been proposed. Their experimental manifestations can be direct, via the production of new particles, or indirect, via deviations of the Higgs properties from their SM predictions.

With its extraodinary energy and integrated luminosity, a 100 TeV pp collider would provide an unprecedented potential to explore in detail the Higgs boson properties, uniquely complementing the capabilities at the LHC and possible future e^+e^- colliders. This note is dedicated to describing this potential.

Section 2 of this note discusses the potential for measuring Higgs properties using single Higgs production. We have been focussing on measurements where the FCC-hh will be able to make the difference compared to the HL-LHC [10] and the FCC-ee [11]. The large statistics available at the FCC-hh allow to select specific region of the phase-space in which the S/B-ratio is large, and where systematics can be kept under control. We will also discuss prospects for measuring the scattering of the longitudinal component of vector bosons, as an indirect probe of the interaction of the Higgs to vector bosons.

Section 3 addresses the determination of the Higgs self-coupling. This measurement is crucially important for several reasons. In the SM, the shape of the Higgs potential is completely fixed by the mass and vacuum expectation value of the Higgs field. Therefore, a measurement of the trilinear Higgs self-interaction provides important additional tests of the validity of the SM and possibly on the origin of the shape of the Higgs potential. The Higgs self-coupling can be accessed through double Higgs production at hadron colliders. We will discuss this measurement in several decay channels and will show that the FCC-hh can provide the single most precise measurement among all proposed future experiments (with a precision of $\approx$ 5%) of this important quantity.

All studies were performed using samples of simulated Monte Carlo events generated with the MG5-aMC@NLO [12] package, showered and hadronized with PYTHIA8 [13]. The detector simulation has been performed with the fast simulation tool DELPHES [14] using the reference FCC-hh detector parameterisation [15, 16]. The analyses presented in what follows are still rather crude when compared to the LHC standards, but have been helpful to define targets for the ultimate attainable precision and the overall detector performance.

2 Higgs and Electroweak Symmetry Breaking

The strength of the Higgs interaction to SM particles have only been measured with limited precision with the current the Run II LHC dataset [17, 18]. Even after the full High Luminosity LHC (HL-LHC) run with the full $\mathscr{L} = 3$ ab^{-1} dataset, the measurements of Higgs couplings to second generation fermions (in the $H \to \mu^+\mu^-$ channel for example) will remain statistically limited [10]. In addition, the FCC-ee will not be able to improve the HL-LHC sensitivity in these channels due to the limited number of produced Higgs bosons [19].

At $\sqrt{s} = 100$ TeV, the Higgs production rate increases by a factor 16 for gluon-fusion production (ggF) with respect to $\sqrt{s} = 14$ TeV, as shown in Table 1. Assuming a total integrated luminosity of $\mathscr{L} = 30$ ab^{-1} at the FCC-hh, we expect $\mathscr{O}(100)$ increase in the number of Higgs events compared to HL-LHC, leading to an overall reduction of $\mathscr{O}(10)$ of statistical uncertainties. The large rates will thus enable precise measurements of branching ratios for rare decay channels.

The case is somewhat similar for the top-Higgs coupling, that despite its large nominal value (due to

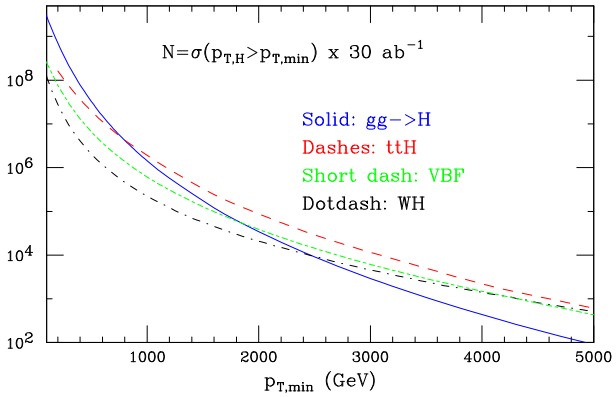

Figure 1: Production rates of Higgs bosons at high p_T, for various production channels at 100 TeV and $\mathscr{L} = 30$ ab^{-1}.

the large top mass), will also be a statistically limited measurement at HL-LHC since it has to be derived from the associated Higgs production with a $t\bar{t}$ pair production rate, which is two orders of magnitude smaller than gluon fusion production at the LHC. At the FCC-hh the ttH rate increases by factor 52 with respect to the LHC, giving a total rate similar to gluon fusion production at the LHC (see Table 1).

Figure 1 shows the Higgs rates above a given p_T threshold, for various production channels. It should be noted that these rates remain above the level of one million up to $p_T \approx 1$ TeV. Furthermore, for $p_T(H) > 1$ TeV, the leading production channel becomes $t\bar{t}H$, followed by vector boson fusion when $p_T(H) > 2$ TeV. The huge statistics available at the FCC-hh (see Table 1) together with the large kinematic range can be used to define cuts improving the signal-to-background ratios and the modelling or experimental systematics (thereby "trading" statistics for low systematics). This will allow to improve the measurements that are systematics limited at HL-LHC, such as $H \to \gamma\gamma$. The large rates at high Higgs p_T can also be exploited for constraining the branching ratio of Higgs decaying to invisible exotic particles.

	ggF	VBF	ttH	VH
$\sigma(100\text{TeV})$(pb)	802	69	33	27
$\sigma(100\text{TeV})/\sigma(14\text{TeV})$(pb)	16	16	52	11
N($\sqrt{s} = 100$ TeV, 30 ab^{-1})	25×10^9	2.5×10^9	10^9	7.5×10^8

Table 1: Upper row: Cross sections at $\sqrt{s} = 100$ TeV for the production of a SM Higgs boson in the gluon fusion (ggF), vector boson fusion (VBF), top pair associated (ttH) and Higgs-strahlung (VH) production modes. Middle row: Rate increase at 100 TeV relative to 14 TeV. Lower row: Expected number of Higgs bosons produced with an integrated luminosity of 30 ab^{-1} [20].

2.1 Measurement of Higgs branching ratios

In this section we discuss the prospects for measuring the branching fractions of Higgs decaying in the following channels:

- $H \to \gamma\gamma$
- $H \to ZZ^* \to 4\ell$
- $H \to \mu^+\mu^-$
- $H \to Z\gamma \to \ell^+\ell^-\gamma$

Signal The four main production modes have been considered: gluon fusion production (ggF), vector boson fusion (VBF), top pair associated production (ttH) and Higgs-strahlung (VH). The cross-sections and the expected number of events expected with an integrated luminosity of 30 ab^{-1} at $\sqrt{s} =$ 100 TeV are summarized in Table 1. Signal events were generated at leading order (LO) with up to two extra merged jets using the MLM procedure [21]. All considered diagrams are at tree level except the ggF mode that was generated including the full top mass dependence. The yields are summarized in Table 2 after inclusive K-factors accounting for current calculations have been applied. The Higgs decay branching fractions have been taken from [22].

	$H \to \gamma\gamma$	$H \to 4\ell$	$H \to \mu^+\mu^-$	$H \to \ell^+\ell^-\gamma$
p_T (H) > 0 GeV	50×10^6	3×10^6	5×10^6	2.5×10^6
p_T (H) > 200 GeV	900×10^3	50×10^3	90×10^3	40×10^3
p_T (H) > 500 GeV	100×10^3	6×10^3	10×10^3	5×10^3
p_T (H) > 1 TeV	4000	250	400	200

Table 2: Expected number of Higgs produced in each decay channel for various Higgs transverse momentum thresholds with an integrated luminosity of 30 ab^{-1}.

Backgrounds The irreducible background in the $H \to \gamma\gamma$ channel is QCD di-photon production which includes a large tree level $qq \to \gamma\gamma$ component, generated with up to two merged extra-jets, and a smaller loop-induced component, $gg \to \gamma\gamma$, generated up to one additional merged jet. This background sample has been generated with the following requirements: $p_T^\gamma > 30$ GeV, $|\eta^\gamma| < 5$ and $50 < m_{\gamma\gamma} < 200$ GeV. The LO cross-sections are found to be $\sigma(qq \to \gamma\gamma) = 615$ pb and $\sigma(gg \to \gamma\gamma) = 25$ pb respectively. An overall normalisation using a global K-factor K=2 has been applied to both contributions to account for higher order QCD corrections.

In the $H \to ZZ^* \to 4\ell$ channel, only the 4ℓ background continuum has been considered. It has been generated at tree-level, with up to one extra merged jet and with $p_T^\ell > 4$ GeV, $|\eta^\ell| < 5$ and $50 < m_{4\ell} <$ 200 GeV. The cross-section is found to be 62 fb, including an overall K-factor K=1.6 [2].

In the $H \to \mu^+\mu^-$ and $H \to Z\gamma$ channels the continuum $\mu^+\mu^-$ and $\ell^+\ell^-\gamma$ backgrounds were generated at tree-level, with up to one extra merged jet and with $p_T^{\ell,\gamma} > 20$ GeV, $|\eta^{\ell,\gamma}| < 5$ and $50 < m_{\mu\mu}$ $(m_{\ell\ell\gamma}) <$ 200 GeV. The cross-section for these processes are $\sigma(\mu^+\mu^-) = 200$ pb, with K=1.2 assumed equal to the Drell-Yan production K-factor, and $\sigma(\ell^+\ell^-\gamma) = 2$ pb with K=1.5.

Contributions from object mis-identification (fakes) were neglected. In the $H \to \gamma\gamma$ channel for instance, the light jets in the γ+jets background (mostly coming from π^0 in jets) could be mis-identified

[2] This value for the K-factor is chosen equal to the inclusive ZZ production at $\sqrt{s} = 100$ TeV [23].

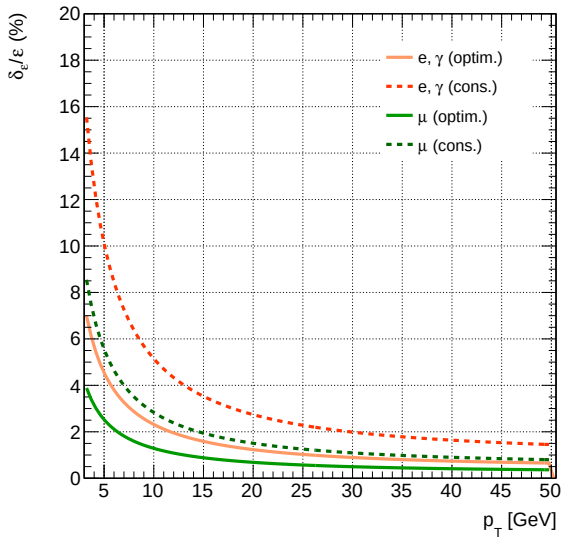

Figure 2: The uncertainty on the reconstruction efficiency of electrons, photons and muons as a function of transverse momentum. An optimistic (solid) and a conservative (dashed) scenario are considered.

as photons. At present LHC experiments, after applying all identification and isolation criteria, the fake background contribution in this decay mode constitutes at most 25% of the total background contribution. We therefore assume this contribution to be included in our conservative K-factor.

Proposed measurements The results are expressed in terms of precision on the signal strength defined as $\mu = \sigma_{\text{obs}}/\sigma_{\text{SM}}$. In the decay channels considered here, the Higgs decay products are visible in the detector and thus the full Higgs invariant mass can be reconstructed. As highlighted in the introduction, the analyses presented here focus on a specific phase space region where the impact of systematic uncertainties tied to reconstruction efficiencies are small. A key observable to define such region is the transverse momentum of the Higgs p_{T} (H), that can be reconstructed completely via the visible decay products.

Physics objects at high p_{T} are typically measured with a high precision, due to reduced mis-identification contributions (fakes) and a smaller relative impact of pile-up. Moreover the accuracy for estimating reconstruction efficiencies typically suffer at low p_{T} from the vicinity to trigger thresholds and from lack of clean data samples for measuring such efficiencies in data. To overcome such issues one has to rely on Monte Carlo simulation, hence increasing the impact of modelling in the total uncertainty. At the FCC-hh, huge control samples will be available at high momenta and will allow for very precise measurements of reconstruction efficiencies in high purity data samples. For instance, electron and muons will be measured from Drell-Yan, both at threshold and in the boosted regime (in order to cover the full kinematic range). Likewise, photon efficiencies will be controlled from abundant and very clean data samples of $\text{Z} \to \mu^+\mu^-\gamma$. The precision of these measurements is nowadays statistics-limited at the LHC. Finally, the use of high-p_{T} Higgs decays allows to minimize the acceptance modeling uncertainties for the production in common fiducial volumes, when extracting ratios of branching ratios for different final states.

Event selection and signal extraction Only minimal optimisation of the selection has been performed. Acceptance cuts for isolated electrons, muons and photons aimed at maximizing the S/B-ratio are applied followed by a requirement on the invariant mass constructed from the Higgs decay candidates

$H \to \gamma\gamma$	$H \to 4\ell$	$H \to \mu^+\mu^-$	$H \to \ell^+\ell^-\gamma$
$p_T^{max}(\gamma) > 30$ GeV $p_T^{min}(\gamma) > 25$ GeV	$p_T^{(1)}(\ell) > 20$ GeV $p_T^{(2)}(\ell) > 10$ GeV $p_T^{(3)}(\ell) > 7$ GeV $p_T^{(4)}(\ell) > 5$ GeV	$p_T^{max}(\mu) > 20$ GeV $p_T^{min}(\mu) > 20$ GeV	$p_T^{max}(\ell) > 20$ GeV $p_T^{min}(\ell) > 20$ GeV $p_T(\gamma) > 15$ GeV
$\lvert\eta(\gamma)\rvert < 4$	$\lvert\eta(\ell)\rvert < 4$	$\lvert\eta(\mu)\rvert < 4$	$\lvert\eta(\ell,\gamma)\rvert < 4$
rel.Iso(γ) < 0.15	rel.Iso(ℓ) < 0.4	rel.Iso(μ) < 0.4	rel.Iso(γ) < 0.15 rel.Iso(ℓ) < 0.4
	$m_{\ell\ell}^{(1)} \in [40,120]$ GeV $m_{\ell\ell}^{(2)} \in [12,120]$ GeV		$m_{\ell\ell} \in [75,105]$ GeV
$\lvert m_{\gamma\gamma} - m_H\rvert < 2$ GeV	$\lvert m_{4\ell} - m_H\rvert < 1$ GeV	$\lvert m_{\mu\mu} - m_H\rvert < 1$ GeV	$\lvert m_{\ell\ell\gamma} - m_H\rvert < 2$ GeV

Table 3: Summary of the event selection criteria used for each channel

to be compatible with m_H = 125 GeV. The relative isolation is computed using the momentum sum of particle-flow candidates [24] inside a cone of size R = 0.3 around the reconstructed particle (excluding the particle itself) divided by the particle p_T.

The event selection for the $H \to \gamma\gamma$ and $H \to \mu^+\mu^-$ requires at least two isolated photons or opposite sign muons. For the $H \to ZZ^* \to 4\ell$ channel, at least four leptons with two opposite sign and same flavour pair are required. One pair is required to have kinematics compatible with an on-shell Z decay, while the other is allowed to be largely off-shell with a small $m_{\ell\ell}$. For the $H \to Z\gamma \to \ell^+\ell^-\gamma$ channel, an isolated photon and only one opposite sign and same flavour pair compatible with an on-shell Z decay is allowed. Further details of the event selection can be found in Table 3. The Higgs invariant mass distributions used for signal extraction are shown in Figures 3 and 4 (left).

Systematic uncertainties At hadron colliders the ultimate precision on cross-section measurements is typically limited by systematic uncertainties on the production cross section σ_{prod} and the integrated luminosity $\mathscr{L}$.

The current uncertainty on the Higgs production cross-section is $\sim 3\%$ [25] dominated by uncertainties on the parton distribution function, α_S and scale uncertainties. We assume that improvements in the theoretical predictions within the timescale of the FCC will result in $\delta\sigma_{prod} < 1\%$. LHC analyses assume luminosity uncertainties of $\delta\mathscr{L} \approx 2.5\%$ [26], here we assume that novel techniques can improve this systematics to $\delta\mathscr{L} \approx 1\%$.

Systematic uncertainties also enter due to object reconstruction efficiencies. The uncertainties for single muon, electron and photon are shown in Figure 2. A conservative and an optimistic scenario are considered. For example, at asymptotically high momenta respectively $\delta_\varepsilon(e,\gamma) = 0.5\%$ and $\delta_\varepsilon(\mu) = 0.25\%$ for the optimistic and $\delta_\varepsilon(e,\gamma) = 1.0\%$ and $\delta_\varepsilon(\mu) = 0.50\%$ for the conservative scenarios. We assume that the uncertainties for electrons and photons are equal and fully correlated, but uncorrelated to those for the muons.

The normalisation of the backgrounds for all channels is determined from control regions defined away from the Higgs mass peak. We therefore assume a negligible uncertainty on the background yield.

Individual channel results The expected precision on the signal strength is given in Figures 3 (right) and 4 (right) as a function of the minimal requirement on the reconstructed Higgs p_T obtained in the $H \to \gamma\gamma$, $H \to 4\ell$, $H \to \mu^+\mu^-$ and $H \to \ell^+\ell^-\gamma$ channels. The expected precision is given for

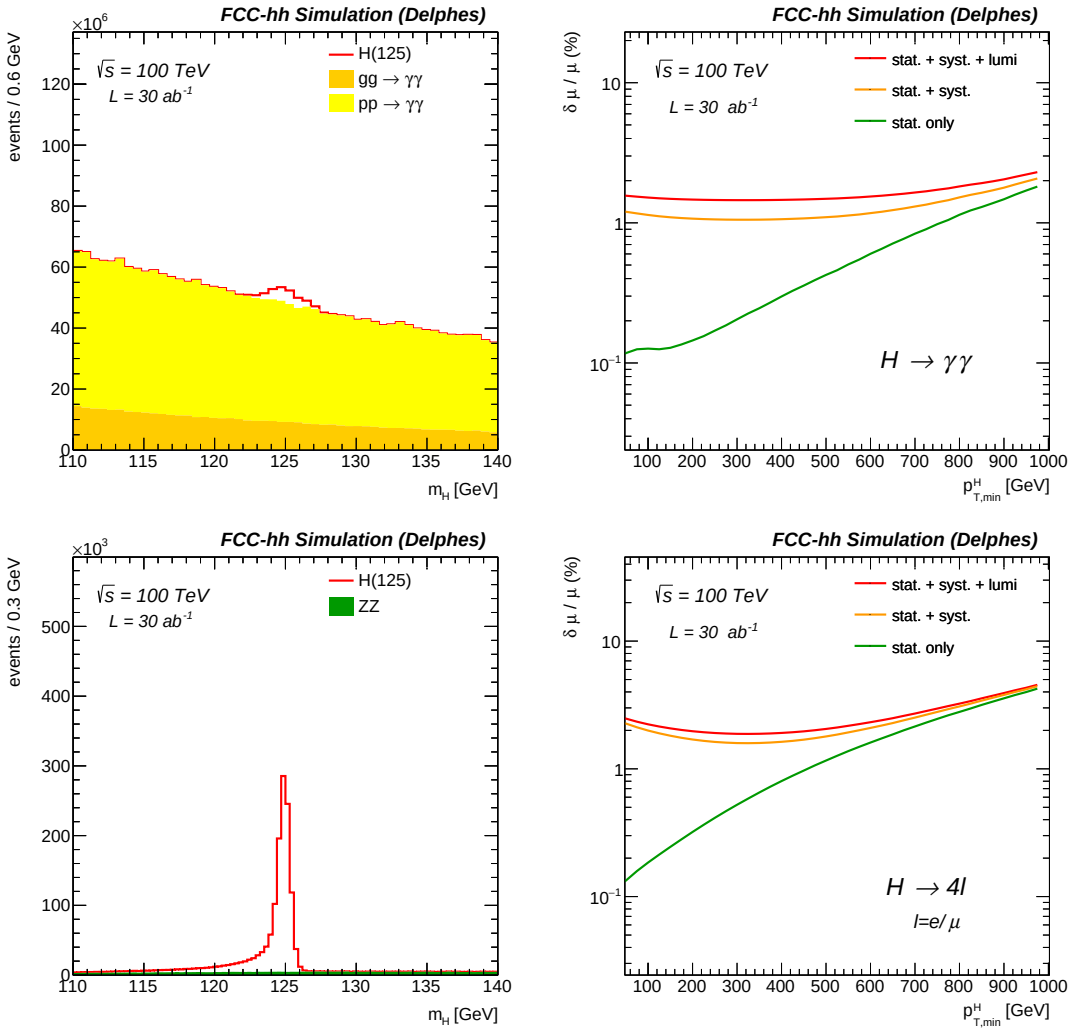

Figure 3: Left: Invariant mass spectrum of the reconstructed Higgs candidate in the $H \to \gamma\gamma$ (top) and $H \to 4\ell$ (bottom) channels, for signal and backgrounds. Right: Expected precision on the signal strength (defined as $\mu = \sigma_{obs}/\sigma_{SM}$) as a function of the minimal requirement on the Higgs reconstructed transerverse momentum obtained in the $H \to \gamma\gamma$ (top) and $H \to 4\ell$ (bottom) channels . The expected precision is given for three scenarios where various assumptions on the uncertainties are made: only statistical uncertainties are included (stat-only), statistical and systematics on the object reconstruction efficiencies (stat. + syst), and statistical, systematics on the object reconstruction efficiencies, and luminosity systematics of $\delta\mathscr{L} \approx 1\%$ (stat + syst + lumi).

three scenarios where various assumptions on the uncertainties are made: only statistical uncertainties (stat-only), statistical plus systematic uncertainties on the object reconstruction efficiencies (stat. + syst), and statistical plus systematics on the object reconstruction efficiencies and luminosity $\delta\mathscr{L} = 1\%$ (stat + syst + lumi). When considering statistical uncertainty only, the expected $\delta\mu/\mu$ does not exceed 1% up to p_T (H) = 200GeV in all channels. When including systematic uncertainties, in particular those related to reconstruction efficiencies, $\delta\mu/\mu$ reaches a miminum for a given p_T^{min}(H). This is because the systematic uncertainty dominates over statistical uncertainty at low momenta, whereas the opposite occurs at high momenta. There is no explicit minimum for the $H \to \mu^+\mu^-$ channel, because this channel becomes statistically limited already at low p_T (H). Depending on the channel and the scenario, the achievable

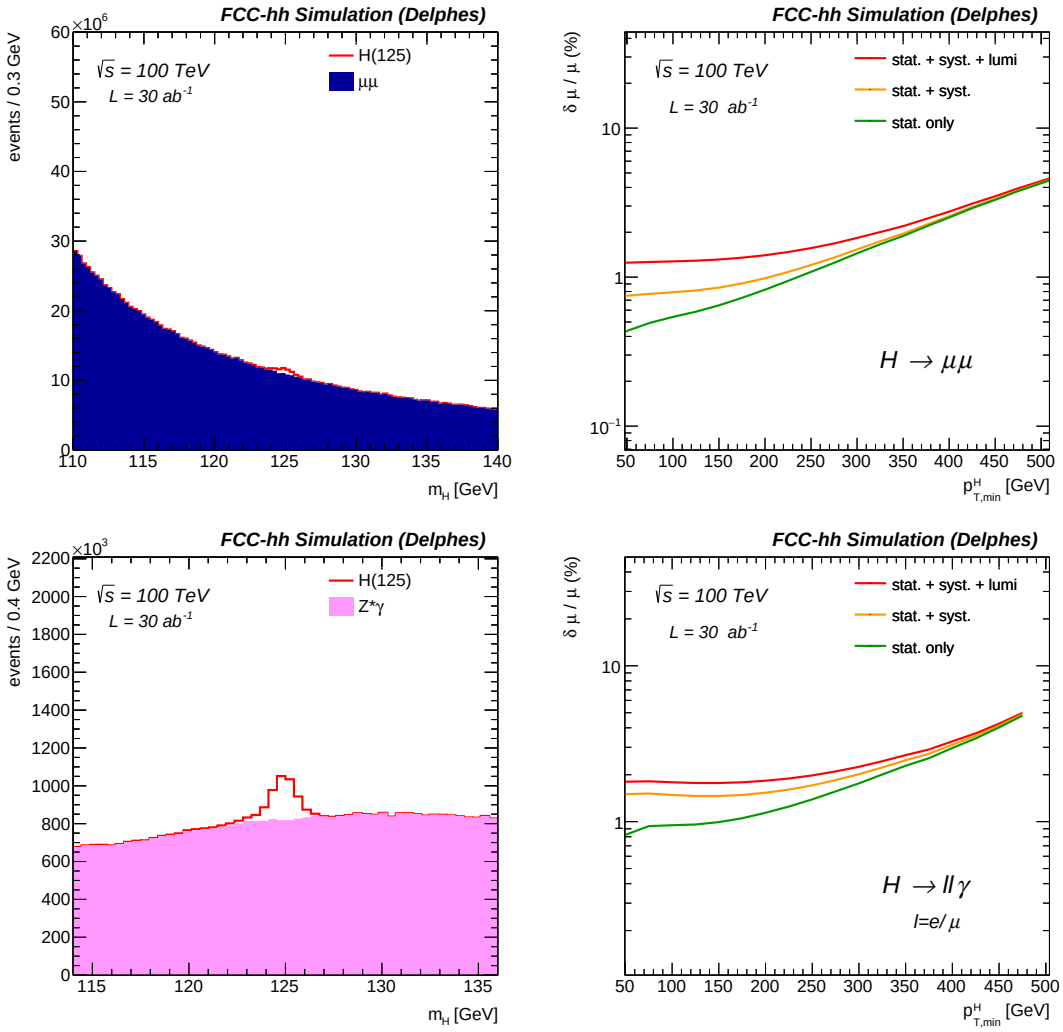

Figure 4: Left: Invariant mass spectrum of the reconstructed Higgs candidate in the $H \to \mu^+\mu^-$ (top) and $H \to \ell^+\ell^-\gamma$ (bottom) channels, for signal and backgrounds. Right: Expected precision on the signal strength (defined as $\mu = \sigma_{obs}/\sigma_{SM}$) as a function of the minimal requirement on the Higgs reconstructed transerverse momentum obtained in the $H \to \mu^+\mu^-$ (top) and $H \to \ell^+\ell^-\gamma$ (bottom) channels. Three scenarios where various assumptions on the uncertainties are shown: only statistical uncertainties are included (stat-only), statistical and systematics on the object reconstruction efficiencies (stat. + syst), and statistical, systematics on the object reconstruction efficiencies, and luminosity measurement systematics of $\delta\mathscr{L} \approx 1\%$ (stat + syst + lumi).

precision on the branching ratio is $\approx$ 1-2%.

Combined results and discussion The results presented in the previous sections can be combined into ratios of couplings, or equivalently of ratio of branching fractions. Given that the fiducial regions for the single channel measurements are defined as function of p_T (H), the relative contributions of production rates across the various channels are preserved. Therefore, the theoretical uncertainties on the production mechanisms, as well as the luminosity uncertainty cancel out in BR(H $\to$ X)/BR(H $\to$ Y) ratios. The precision on such ratios is thus determined by statistics and by efficiency uncertainties. Moreover, in specific ratios such as BR(H $\to \mu^+\mu^-$)/BR(H $\to 4\mu$), BR(H $\to \gamma\gamma$)/BR(H $\to 2e2\mu$) or BR(H $\to \mu\mu\gamma$)/BR(H $\to 4\mu$), the reconstruction efficiency uncertainties partially cancel. The cancel-

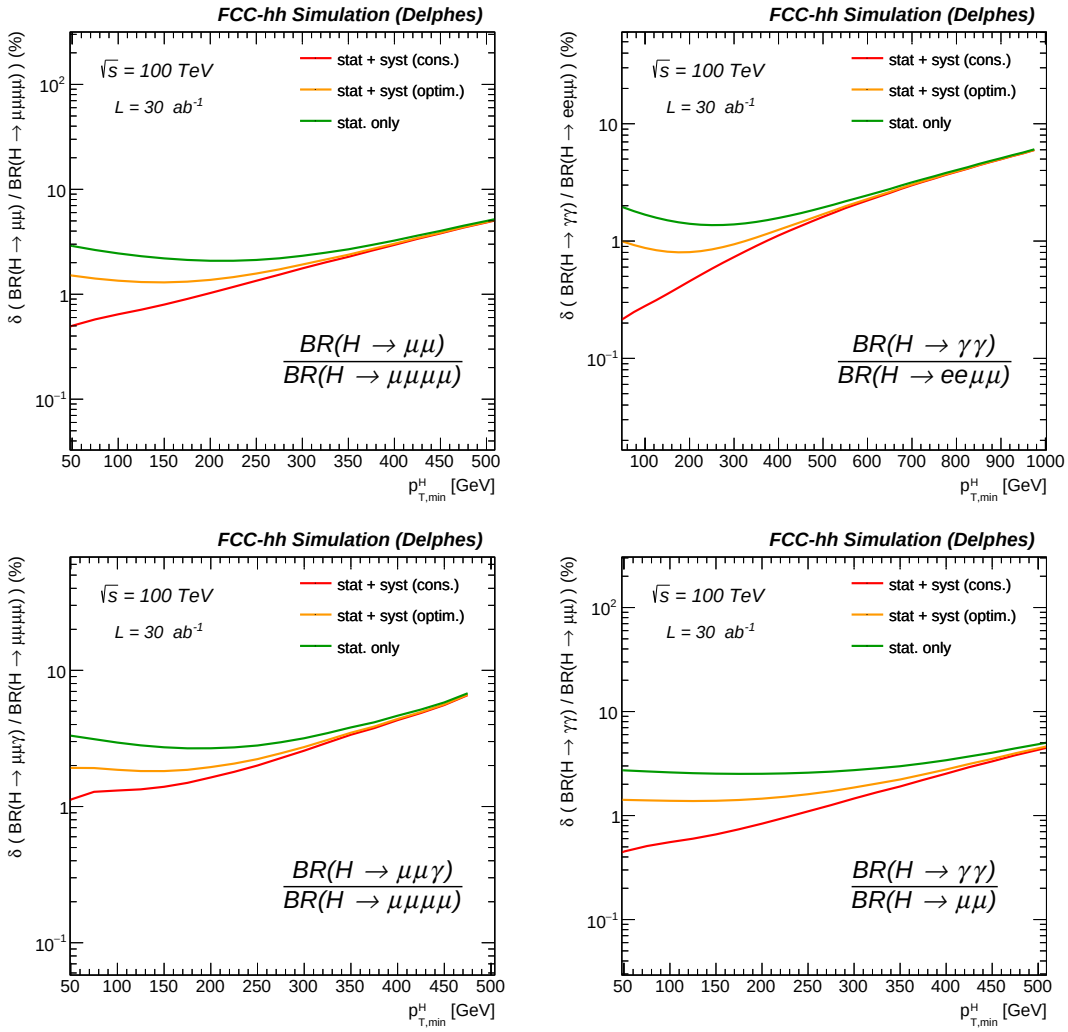

Figure 5: Expected precision on the ratio $\mathrm{BR}(\mathrm{H} \to \mu^+\mu^-)/\mathrm{BR}(\mathrm{H} \to 4\mu)$ (top left), $\mathrm{BR}(\mathrm{H} \to \gamma\gamma)/\mathrm{BR}(\mathrm{H} \to 2e2\mu)$ (top right), $\mathrm{BR}(\mathrm{H} \to \mu\mu\gamma)/\mathrm{BR}(\mathrm{H} \to 4\mu)$ (bottom left) and $\mathrm{BR}(\mathrm{H} \to \gamma\gamma)/\mathrm{BR}(\mathrm{H} \to \mu^+\mu^-)$ (bottom right) as a function of the minimal requirement on the Higgs reconstructed transverse momentum. The expected precision is given for three scenarios where various assumptions on the uncertainties are made: only statistical uncertainties are included (stat-only), statistical and optimistic (conservative) systematics on the object reconstruction efficiencies. All the uncertainties on the production, both theoretical and from luminosity cancel in the ratio.

lation is complete when the uncertainties on the objects are fully correlated (e.g. if the same object appear in the numerator and denominator) and if the kinematics are similar. The expected precision for four such ratios is shown in Figure 5 as a function of the requirement on p_{T} (H). The expected precision is given for three scenarios where various assumptions on the uncertainties are made: only statistical uncertainties are included (stat-only), and statistical plus optimistic (or conservative) systematics on the object reconstruction efficiencies. Roughly, the maximum precision is respectively $\approx 1\%$ (2%) for optimistic (conservative) assumptions. At the FCC-ee, $\mathrm{BR}(\mathrm{H} \to \mathrm{ZZ}^*)$ can be measured with a precision of $\approx 0.2\%$ (see Ref. [19]). Provided that such measurement becomes available before FCC-hh data taking, relative measurements that involve the $\mathrm{H} \to \mathrm{ZZ}^*$ coupling in the denominator can be converted to absolute measurements of the branching fraction involved in the numerator.

2.2 Higgs to Invisible

Introduction An important component of the dark matter search is the search for the Higgs decaying to invisible particles. For a large class of models [27–31], the Higgs boson can act as a portal between matter and dark matter. In these models, the Higgs is capable of interacting with both matter and dark matter. In some cases, the Higgs mixes with a dark sector scalar particle and decays to dark sector particles as a result of the mixing. In other cases, the Higgs couples directly to a dark matter particle without any additional particles.

The search for Higgs decaying invisibly uses the $p_{\mathrm{T}}^{\mathrm{miss}}$ distribution since the $p_{\mathrm{T}}^{\mathrm{miss}}$ reflects the p_{T} spectrum of the Higgs boson. The large statistics of Higgs produced at large p_{T}, in the TeV range, allows to search for its invisible decays in an environment where the instrumental $p_{\mathrm{T}}^{\mathrm{miss}}$ backgrounds are suppressed, and the physics ones (e.g. $\mathrm{Z}\rightarrow \nu\bar{\nu}$) can be better controlled.

Multiple Higgs production modes can be used. The total Higgs production cross section is dominated by gluon fusion and vector boson fusion. However, at high p_{T} the relative proportion of gluon fusion with respect to the rest of the other production modes is reduced (see Figure 1), including Higgs produced in association with top quarks and vector boson fusion. The VBF and the $\mathrm{t\bar{t}H}$ both have advantageous properties that allow for further signal background separation.

The VBF production mode has the characteristic signature of two jets with relatively large $|\eta|$ corresponding to additional quarks that result from the emission of W pairs necessary to produce the Higgs boson. With the current 13 TeV searches, the VBF production mode is the dominant channel for the Higgs invisible search. Largely as a result of the quark initial state, the vector boson production mode does not have a significantly different p_{T} spectrum when compared with background processes. Consequently, the most powerful approach to searching for the Higgs invisible decay in this mode is to look for events with large missing transverse energy and large di-jet pair mass m_{jj}. The current 13 TeV search is performed by fitting the dijet mass pair with a $p_{\mathrm{T}}^{\mathrm{miss}}$ requirement above 200 GeV.

The search for Higgs decaying invisibly produced with pairs of top quarks is perhaps the most promising channel since the relative cross section is hugely enhanced with the respect to background processes when compared to 13 TeV Higgs production and the top pair decays allow for a very distinct signature that can significantly reduce the background. In this study, a dedicated analysis isolating Higgs production produced in association with tops is not performed; its addition would likely lead to a further enhancement in sensitivity.

Event Selection Events are required to have large missing energy and no additional leptons including taus. Events are triggered with a missing energy trigger. For this study a trigger that yields 100% efficiency at a $p_{\mathrm{T}}^{\mathrm{miss}}$ value of 200 GeV is required. This choice of trigger is consistent with the current plateau in both the LHC ATLAS and CMS experiments. Projections with the high luminosity upgrade for the LHC also indicate that with the addition of tracking into the level one trigger system, this plateau can be maintained during high intensity running of the LHC.

Backgrounds The main backgrounds consist of Z boson production, where the Z boson decays to neutrinos ($\mathrm{Z}\rightarrow \nu\bar{\nu}$) and W boson production, where the W boson decays leptonically and the lepton is not identified. The lepton is missed either because the lepton transverse momentum is too low (as in the case of $\tau \rightarrow \ell\nu\bar{\nu}$) or the lepton falls out of the acceptance of detectors capable of identifying the lepton (eg. tracking detector and muon chambers for the case of muons). The next largest background consists of top pair production where one of the top quarks decays leptonically and the lepton fails to be identified. This background is very similar to single W boson production with additional jets.

Current monojet analysis in ATLAS and CMS [32, 33] use a series of control regions to precisely predict the backgrounds. The Z boson background where the Z boson decays to neutrinos, is predicted by constructing a control region by selecting electron or muon pairs, consistent with the Z boson decay.

The leptons are then treated as "invisible" and removed from the event to effectively mimic the Z to neutrino topology. The overall shape of these Z events matches the Z to neutrino events very well, excluding the regions where the leptons would not be selected in the detector. The normalization of the Z boson events can then be determined from the data and is limited by the uncertainty in the lepton pair selection efficiency.

W events are selected by requiring a lepton, electron or muon, and missing transverse energy. The lepton is removed from the computation of the $p_{\mathrm{T}}^{\mathrm{miss}}$ so as to match the final $p_{\mathrm{T}}^{\mathrm{miss}}$ selection. These events are then used to predict the shape of the W boson events where the lepton is not selected by adding extrapolation uncertainties characteristic with the accuracy of the lepton rapidity distribution and the lepton efficiency. In addition, W boson events can be used to predict Z boson events and single isolated photon events can be used to predict the background shape of both Z boson and W boson events. To use these events in the prediction, we exploit the fact that the prediction of the production ratios is known to significantly higher precision than the production of the individual processes [34]. This is because W, Z, and photon production have the same QCD production diagrams at leading order in the electroweak production. They differ at higher order electroweak scale. However, their differences have been characterized leading to a predicted uncertainty in the production modes that varies from 1-5% as a function of the single boson p_{T}.

Monte Carlo Samples The generation of Z events includes all instances where a Z boson decays to neutrinos, including both diboson production and single Z production. W boson events include both single boson and diboson production occur as long as there is one leptonically decaying W boson. W and Z boson events are generated at NLO with up to 2 jets and merged followed the FxFx merging prescription [35]. Top pair events are generated separately at NLO with up to one additional jet and at least one top is required to have a W boson decaying leptonically. Electroweak production of W and Z boson through vector boson fusion is generated separately at LO. These processes consist of W and Z boson merged events, which can produce a single boson. Such backgrounds are necessary when trying to characterize the sensitivity to vector boson fusion since they constitute the largest irreducible backgrounds.

Signal extraction and results The signal is extracted using a simultaneous fit of all background control regions is performed using the same Monte Carlo where the total number of Monte Carlo events is fixed to a specific luminosity choice. The luminosity is then scanned ranging from 1 fb^{-1} to the full 30 ab^{-1}. At each luminosity point the asymptotic limit is extracted using the fit with all control regions. The performance is examined considering multiple systematic uncertainty approaches:

- **Experimental Systematics:** The driving experimental systematic uncertainties originate from the extrapolation from the control regions to the signal region. For W boson and top events falling in the signal region, a lepton must not be found within the signal region acceptance. The leading uncertainty is the uncertainty on the lepton efficiency. We assume a lepton efficiency uncertainty of 0.5%, 0.25%, and 5% for the electron, muon, and hadronic taus respectively. We assume a luminosity uncertainty of 1%. It should be noted that such experimental systematics will dominate in the large integrated luminosity regime ($\approx$ 1 ab^{-1}). At low integrated luminosity, where the statistics of $\mathrm{Z}\to\ell\ell$ control samples at large Z p_{T} are small, the extrapolation from control to signal region will be performed using theory predictions (mainly from γ+jets, see next bullet).

- **"Conservative/default" Theoretical Systematics:** When performing the signal extraction, the uncertainties on the fit are driven by the uncertainty on the ratio of the production of single bosons. To simplify the implementation we take three sets of uncertainties: an increasing slope going from 5% at a p_{T} = 0 GeV to 15% at a p_{T} = 3TeV, which mimics the NLO electroweak correction shape; a flat uncertainty of 8%, which matches the orthogonal eigen-component of the factorization and

renormalization scales and a 5% uncertainty at a p_T = 0 GeV that then goes to a negative 5% uncertainty at a p_T = 3 TeV. Each suite of three uncertainties are combined for each respective process production ratio W/Z and γ/Z. Again, we stress that such uncertainties from theoretical predictions have a sizable effect only in the low integrated luminosity regime, where the statistics from Z$\to \nu\bar{\nu}$ are small.

- **"Aggressive/1%" Theoretical Systematics:** The same uncertainty scheme as the previous one is used except now the uncertainty is reduced by an order of magnitude.

Figure 6 shows the sensitivity of the Higgs boson to invisible branching ratio as a function of luminosity for several uncertainty schemes. Either approach to the theoretical uncertainties appears to be sub-dominant to the impact of the experimental uncertainties. In all cases, however, the uncertainties continue to scale with $\sqrt{\mathscr{L}}$. With $\mathscr{L} = 30$ ab^{-1}, we reach a branching ratio of the Higgs boson to invisible of 10^{-4}. This is well below the SM branching ratio of the Higgs boson to neutrinos BR(H$\to$ ZZ$\to \nu\nu\nu\nu$) $\approx 10^{-3}$ and consequently we would be able to observe a signal which would look very much like an actual dark matter signature. No actual loss in sensitivity is incurred by the observation of the SM production because we assume that the SM production rate is known. The signal was extracted either from the p_T^{miss} distribution or from a two category extraction where in the one jet exclusive category the p_T^{miss} is fit while for events with at least two jets the two highest p_T jets are combined and their dijet mass m_{jj} are fit. The two category extraction enhances the sensitivity to VBF production. In both scenarios, the sensitivity is within 20% of each other and the scaling with respect to the luminosity is roughly the same.

The results are translated to compare to direct detection results following [36]. Figure 6 shows that a result comparable to that of the expected ultimate limit of direct detection as defined by the bound induced from neutral current neutrino interactions known as the neutrino floor.

In summary, by performing a simultaneous fit of the hadronic recoil (e.g. p_T^{miss}) spectra of five control regions defined by Z and W to lepton decays and γ+jets it is possible to constrain both theory and experimental systematics to obtain an extremely precise prediction of the Z$\to \nu\nu$ spectrum. This simultaneous fit is used to probe the decay of the Higgs to invsible particles. The resulting sensitivity shows a sensitivity to a branching ratio of the Higgs to invisible particles of roughly 10^{-4}; a bound that is sensitive to the SM H$\to \nu\nu\nu\nu$ and which extends to the maximal bound of the direct detection searches.

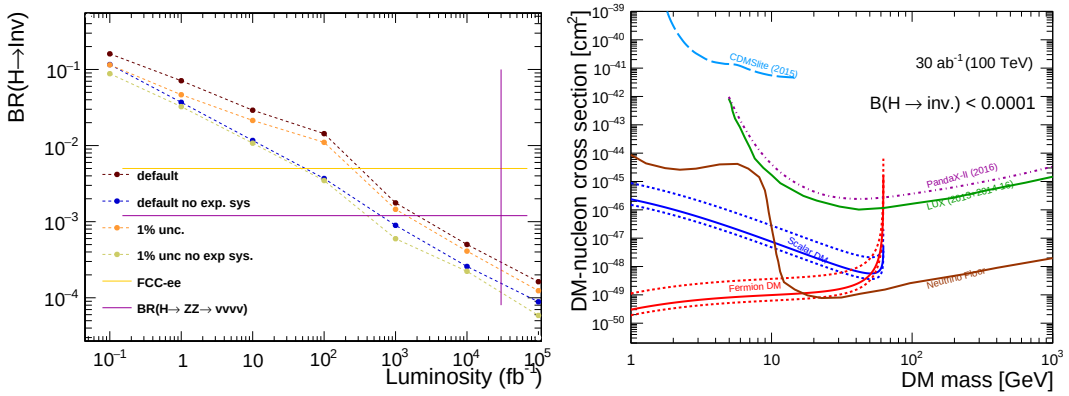

Figure 6: (Left) Expected limit as a function luminosity for the Higgs to invisible for multiple uncertainty schemes. (Right) Translation of limit at 30 ab^{-1} to the direct detection plane and comparison with LUX [37], PandaX-II [38], CDMSLite [39], and the neutrino floor[40].

2.3 The Top Yukawa

The coupling of the Higgs with the top quark y_t is a crucial parameter of the SM. In contrast to other Yukawa couplings that can be assessed via Higgs decay rates, the largest direct sensitivity can be obtained via the ttH production mechanism. The ttH production mode was recently observed at the LHC [41, 42]. Due to the small production rate (only 1% among the Higgs bosons produced at the LHC are produced via ttH), y_t is expected to be measured with a precision of $\approx 3.4\%$ by the end of HL-LHC program [10]. Given the large Q^2 of the ttH production mode, the cross-section increases by a factor ≈ 55 from $\sqrt{s} = 14$ TeV to $\sqrt{s} = 100$ TeV (see Table 1). There are a number of Higgs decay channels which can be used to study ttH production, including $H \to \gamma\gamma$, $H \to b\bar{b}$ and Higgs decays to leptons. Here we focus on the $t\bar{t}H$, $H \to b\bar{b}$ (boosted) channel, following the approach outlined in Ref. [43].

The idea is to measure the ratio of the rates of the two processes ttH and ttZ in the $H \to b\bar{b}$ and $Z \to b\bar{b}$ decay modes respectively. The quantity $\sigma_{ttH}/\sigma_{ttZ}$, or equivalently $\alpha = N(ttH)/N(ttZ)$ (where N is the number of events after some selection) allows to exploit the similarity and thus the cancellation of the dominant sources of uncertainties in the numerator and the denominator. The similarity between the diagrams and energy scales for ttH and ttZ production will ensure that most theoretical uncertainties will cancel out [43]. Likewise, experimental uncertainties such as the luminosity uncertainty and, due to similar kinematics between the $Z \to b\bar{b}$ and $H \to b\bar{b}$ final states, uncertainties on the object selection also cancel out to a large extent.

We focus on the final state where one top decays leptonically, the other top decays hadronically and the Higgs to decay to a $b\bar{b}$ pair. The combinatorial backgrounds are reduced, by focussing on the "boosted topology" where the Higgs boson is produced with large transverse momentum. The final state is therefore characterized by one isolated high p_T lepton, two large radius jets that contain the boosted hadronic top and the higgs, an additional heavy flavour jet (b-tagged) and large missing transverse energy p_T^{miss}.

Monte Carlo Events The ttH and ttZ samples were generated at LO with up to one extra merged jet. Predictions of NLO cross sections of $\sigma_{ttH} = 34$ pb [20] and $\sigma_{ttZ} = 64.2$ pb [23] were used. The $t\bar{t}$+jets background was generated at LO in two separate components: the reducible $t\bar{t}$+jets contribution in the 4-flavour (4F) scheme and the irreducible $t\bar{t}b\bar{b}$ contribution. Both components were generated with a $p_T^{t\bar{t}} > 150$ GeV requirement at generation level. In order to account for higher order QCD corrections a K-factor (K=1.4) derived from inclusive $t\bar{t}$ production has been applied. The cross-sections obtained with the described setup are $\sigma_{t\bar{t}+jets} = 6.75$ nb and $\sigma_{t\bar{t}b\bar{b}} = 120$ pb. The W+jets background is negligible.

Event selection Jets are clustered from particle-flow candidates with the anti-k_T algorithm [44] with a radius parameter R=1.5. A large fraction of the Higgs and top decay products are included in the jet, hence the denomination "fat-jets". Events are first pre-selected by requiring at least two central fat jets with $p_T^j > 250$ GeV and $|\eta^j| < 3.0$ that contain at least two subjets with R=0.4, and at least one central isolated lepton with $p_T^\ell > 25$ GeV and $|\eta^\ell| < 3.0$.

The fat-jets containing the smallest and largest number of sub-jets are labeled as the "Higgs-jet" and "Top-jet" respectively. If the number of sub-jets is equal, the fat-jets are ranked according to the soft-dropped mass m_{SD} [45] and the fat-jet with the smallest (largest) m_{SD} is labeled the Higgs-(Top-)jet.

Fat-jets containing the Higgs or top decay products, typically feature two-prong or three-prong structures, in contrast to QCD jets from the $t\bar{t}$+jets background that contain on average one subjet. The difference in the "2" versus "1" prong hypotheses of a jet is exploited with the $\tau_{2,1}$ observable [46] and used to further increase the signal purity in Higgs-jet candidates. Similarly a $\tau_{3,2}$ selection can exploit the difference in the "3" versus "2 or less" sub-jets hypotheses. The Top-jet candidate is required to pass the criteria $120 < m_{SD}^{top} < 250$ GeV and $\tau_{3,2} < 0.8$ while the Higgs-jet is only required to pass the $\tau_{2,1} < 0.6$ criterion. Given that m_{SD}^{H} is used for the signal extraction, no selection is applied on this observable. Finally, in order to further reject the large $t\bar{t}$+jets background, at least 4 b-tagged jets are required.

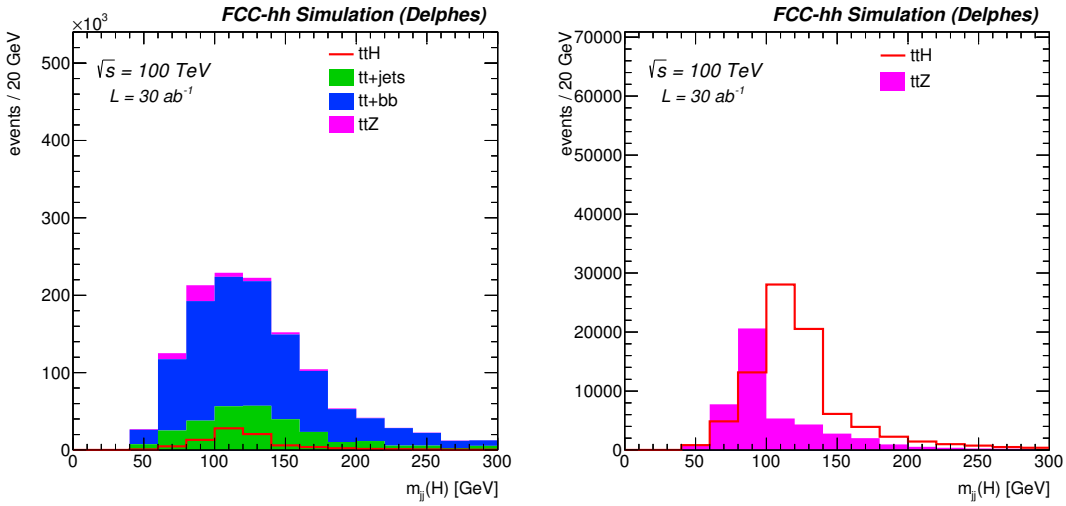

Figure 7: Invariant mass the di-jet pair forming the Higgs candidate including all backgrounds (left) and after (perfect) background subtraction as input for measuring the ttH/ttZ fraction (right).

Signal extraction and results The ttH and the ttZ contributions are simultaneously extracted by fitting the di-jet invariant mass spectrum shown in Figure 7. Our signal model is a linear combination of ttH and ttZ templates where the ttH and ttZ yields are the parameters of interest. The $t\bar{t}$+jets and $t\bar{t}b\bar{b}$ backgrounds yields are measured with a negligible statistical uncertainty from a control sample defined by the $m_{b\bar{b}} > 200$ GeV event selection criterion. We find $\mathrm{N(ttH)/N(ttZ)} = 1.64 \pm 0.01$ (stat.) that leads to an overall precision on the Yukawa coupling of $\delta y_t / y_t \approx 1\%$. This assumes that the theoretical prediction on $\mathrm{N(ttH)/N(ttZ)}$ (inclusive and differential) will have similar precision [23] and that the ttZ coupling will be known with a precision of 1%, possibly thanks to the FCC-ee run at the $t\bar{t}$threshold. We note that in this study we neglected the impact of the modelling of the background shape on the determination of $\mathrm{N(ttH)/N(ttZ)}$. Further studies to assess this effect will need to be carried out.

2.4 Vector Boson Scattering

Introduction In the absence of the Higgs boson in the Standard Model (SM) the scattering of longitudinally polarized vector bosons ($\mathrm{V_L V_L}$ scattering where V=W,Z) is divergent at high energy and violates unitarity. In particular, if the couplings of the Higgs boson to vector bosons deviate from the SM value, the delicate balance that preserves unitarity can be spoiled and lead to large enhancements in VV scattering at high energy, potentially providing hints of new physics. Vector boson scattering (VBS) at high energies can therefore help to elucidate the nature and the mechanism of electro-weak symmetry breaking (EWSB) in a model independent way. At hadron colliders VBS occurs via the reaction $\mathrm{qq} \rightarrow \mathrm{VVjj}$. Due to the absence of colour exchange, the final state typically features the presence of two very forward jets, with very little central activity. The average pseudo-rapidity of the most forward jet is $|\eta| \approx 4.5$ at $\sqrt{s} = 100$ TeV compared to $|\eta| \approx 3.5$ at $\sqrt{s} = 14$ TeV.

VBS processes can be studied in several channels but we focus here only on the $\mathrm{W^{\pm}W^{\pm}}$ same sign production, which provides the largest S/B. Projections for the HL-LHC indicate an expected signficance of 3σ for the $\mathrm{W_L W_L}$ discovery after 3 $\mathrm{ab^{-1}}$ [47]. Thanks to large increase in rate at $\sqrt{s} = 100$ TeV the FCC-hh will allow for a measurement the $\mathrm{V_L V_L}$ process at the percent level.

In this document, we explore the prospects of measuring the longitudinal $\mathrm{W_L^{\pm}W_L^{\pm}}$ VBS cross section at the FCC-hh. The robustness of the sensitivity as a function of various scenarios of detector acceptance is also discussed. The VBS process does in principle interfere with other electro-weak and QCD production

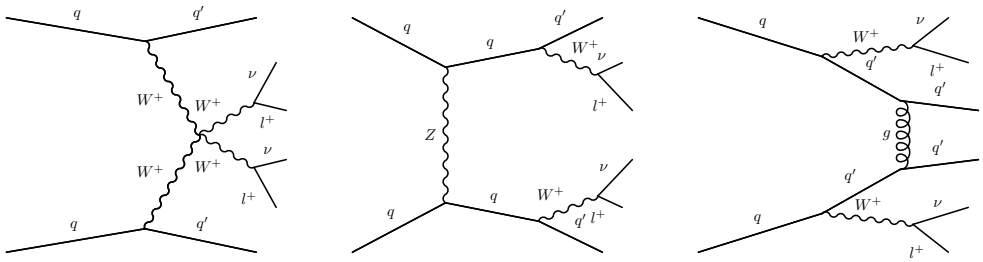

Figure 8: Representative Feynman diagrams for Vector Boson Scattering (left), EWK t-channel production (center) and QCD (right) $W^{\pm}W^{\pm}jj$ production.

$W^{\pm}W^{\pm}$ mechanisms (see Figure 8), however the interference between EWK and QCD is very small and can be neglected. In the fully leptonic mode this channel features two same sign leptons in addition to the characteristic forward jets. The main prompt backgrounds for same sign leptons are $W^{\pm}W^{\pm}$ (QCD) and WZ+jets production. Other potential backgrounds such as non-prompt backgrounds coming from $t\bar{t}$, WW and double parton scattering are neglected in this study.

Signal and background events The electro-weak $pp \to W^{\pm}W^{\pm}qq \to \ell^{\pm}\nu\ell^{\pm}\nu qq$ sample was generated at LO for the three polarisations (TT,TL and LL) components separately. Fiducial requirements were applied in the generation to increase the generation efficiency. Both partons were required to have $p_{\mathrm{T}} > 20$ GeV and $|\eta| < 6$. We also require a rapidity gap $\Delta\eta_{qq} > 2.5$ and a large di-jet invariant mass $m_{qq} > 200$ GeV to enhance the VBS contribution. The total fiducial cross-section for this process at $\sqrt{s} = 100$ TeV is $\sigma(W^{\pm}W^{\pm}jj)^{EWK} = 0.39$ pb. The composition in LL component is around 10%. Since the interference with the EWK contribution is small, the QCD contribution was generated in a separate sample with the same selection at generator level. The LO cross section for this process is $\sigma(W^{\pm}W^{\pm}jj)^{QCD} = 0.17$ pb. Finally the WZ contribution was generated at LO with up to 2 jets merged. The inclusive cross-section $\sigma(WZ) = 611$ pb was used, including a K=1.7 to account for higher order corrections [23].

Event selection and signal extraction We require at least two same-sign leptons (electrons and muons) with $p_{\mathrm{T}}^{\ell} > 20$ GeV and $|\eta_{\ell}| < 4$. The relative isolation is computed using the momentum sum of particle-flow candidates [24] inside a cone of size R = 0.3 around the reconstructed particle (excluding the particle itself) divided by the particle p_{T}. We then require at least two jets with $p_{\mathrm{T}}^{j} > 30$ GeV and $|\eta_{j}| < 6$ reconstructed with the anti-k_T [44] algorithm with a parameter $R = 0.4$.

Specific cuts designed to enhance the VBS topology contribution relative the other EWK and QCD $W^{\pm}W^{\pm}jj$ contributions are then applied. Events with a large di-jet invariant mass $m_{\mathrm{jj}} > 600$ GeV and rapidity gap between the two leading jets $\Delta\eta_{\mathrm{jj}} > 3.5$ GeV are selected. We reduce substantially the WZ background by vetoing events with the presence of an additional lepton and require $p_{\mathrm{T}}^{\mathrm{miss}} > 50$ GeV as well as $m_{\ell\ell} > 50$ GeV.

Figure 9 shows the WZ and the $W^{\pm}W^{\pm}$ QCD background contributions to three key observables together with the total EWK contribution normalized to $\mathscr{L} = 30$ ab^{-1}. Figure 9 (left) shows the di-jet invariant mass. The center plot shows the dilepton invariant mass distribution, as a proxy for the WW invariant mass. Several thousands of events will be available at large diboson mass to probe the unitarization of the vector boson scattering. In Figure 9 (right) we shown the pseudo-rapidity distribution of the most forward jet.

Two observables are used for the signal extraction. The azimuthal angle between the two leptons $\Delta\phi_{\ell\ell}$ discriminates between the LL and TT/TL polarisations as can be seen in Figure 10 (left). The leading jet rapidity discriminates against the large WZ+jets and the $W^{\pm}W^{\pm}$ QCD backgrounds. The extraction

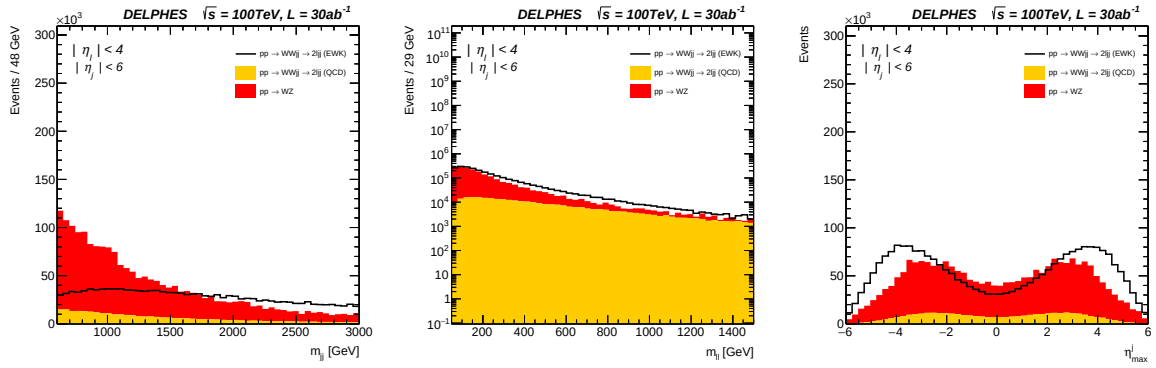

Figure 9: Distributions of the di-jet (left), di-lepton (center) invariant mass and pseudo-rapidity of the most forward reconstructed jet (right). The background contributions WZ and $W^{\pm}W^{\pm}$ (QCD) are stacked, while the $W^{\pm}W^{\pm}$ (EWK) process is not.

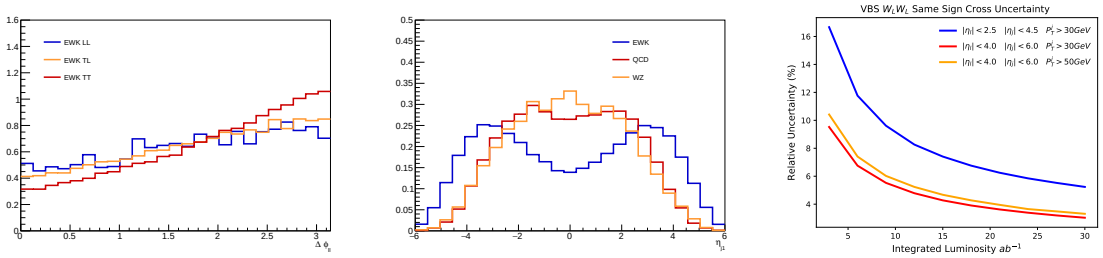

Figure 10: Left: The distribution azimuthal angle between the two leptons $\Delta\phi_{\ell\ell}$ for the 3 polarisations components (TT,TL and LL) of the $W^{\pm}W^{\pm} \to \ell^{\pm}\nu\ell^{\pm}\nu$ process. Center: The distribution of the leading jet pseudo-rapidity for the inclusive $W^{\pm}W^{\pm} \to \ell^{\pm}\nu\ell^{\pm}\nu$ (EWK) signal sample and the $W^{\pm}W^{\pm} \to \ell^{\pm}\nu\ell^{\pm}\nu$ (QCD) and WZ+jets backgrounds. Right: Relative uncertainty of the same-sign $W^{\pm}W^{\pm}$scattering as a function of the integrated luminosity.

of the longitudinal component of the $W^{\pm}W^{\pm}$ (EWK) process is performed via a 2-dimensional fit of these two observables using templates for each polarisation component and assuming that the TT, TL components will be known (possibly from opposite sign WW scattering). The fit uncertainties are driven by an uncertainty of 10% on shapes , 1% on luminosity , 1% on the parton distribution functions and 0.5% on lepton efficiency.

Results and discussion The expected relative uncertainty on the same-sign $W_L^{\pm}W_L^{\pm}$ scattering cross-section is shown in Figure 10 (right) as a function of the integrated luminosity. Under the nominal detector assumption (red curve), i.e. with the ability of reconstructing leptons up to $|\eta_\ell| < 4$ and jets up to $|\eta_j| = 6$, this process can be measured with precision of $\approx 2\%$ with the full $\mathscr{L} = 30$ ab^{-1} of FCC-hh program.

We also studied the effect on the sensitivity of a reduced acceptance (similar to that of the LHC experiments) for leptons and jets ($|\eta_\ell| < 2.5$ and $|\eta_j| = 4.5$). With these assumptions the expected precision is degraded to $\approx 6\%$.

With 1000 simultaneous interactions per bunch cross (pile-up events) it may be impossible to accurately reconstruct jets down to $p_T^j > 30$ GeV, in particular in the forward region. We studied the impact of raising this threshold to $p_T^j > 50$ GeV (yellow) and we observe a relatively negligible degradation in the sensitivity. Nevertheless, pile-up rejection in the forward region, for example with the help of timing detectors is essential for the success of this measurement.

2.5 Summary

The prospects for measurements of the Higgs properties are summarized in Table 4, separately showing the statistical and systematic uncertainties obtained in our studies. As remarked above, there is in principle room for further progress, by fully exploiting data-driven techniques to reduce the experimental systematics. At the least, one can expect that these potential improvements will compensate for the current neglect of other experimental complexity, such as pile-up. The most robust measurements will involve the ratios of branching ratios. Taking as a given the value of the HZZ coupling (and therefore BR(H$\to 4\ell$)), which will be measured to the few per-mille level by FCC-ee, from the FCC-hh ratios it could be possible to extract the absolute couplings of the Higgs to $\gamma\gamma$ (0.4%), $\mu\mu$ (0.7%), and Zγ (0.9%).

The ratio with the $t\bar{t}Z$ process is considered for the $t\bar{t}H$ process, as proposed in Section 2.3 and Ref. [43]. Assuming the FCC-ee will deliver the expected precise knowledge of BR(H$\to b\bar{b}$), and the confirmation of the SM predictions for the $Zt\bar{t}$ vertex, the $t\bar{t}H/t\bar{t}Z$ ratio should therefore allow a determination of the top Yukawa coupling to 1%. The limit quoted in Table 4 on the decay rate of the Higgs boson to new invisible particles is obtained from a study of large missing transverse energy signatures was discussed in Section 2.2. The implications of this measurement for the search of dark matter or dark sectors coupling to the Higgs boson are discussed in [11].

Observable	Parameter	Precision (stat)	Precision (stat+syst+lumi)
$\mu = \sigma$(H)×BR(H$\to \gamma\gamma$)	$\delta\mu/\mu$	0.1%	1.45%
$\mu = \sigma$(H)× BR(H$\to\mu\mu$)	$\delta\mu/\mu$	0.28%	1.22%
$\mu = \sigma$(H)×BR(H$\to 4\mu$)	$\delta\mu/\mu$	0.18%	1.85%
$\mu = \sigma$(H)×BR(H$\to \gamma\mu\mu$)	$\delta\mu/\mu$	0.55%	1.61%
$R =$ BR(H$\to\mu\mu$)/BR(H$\to 4\mu$)	$\delta R/R$	0.33%	1.3%
$R =$ BR(H$\to\gamma\gamma$)/BR(H$\to$ 2e2μ)	$\delta R/R$	0.17%	0.8%
$R =$ BR(H$\to\gamma\gamma$)/BR(H$\to 2\mu$)	$\delta R/R$	0.29%	1.38%
$R =$ BR(H$\to\mu\mu\gamma$)/BR(H$\to\mu\mu$)	$\delta R/R$	0.58%	1.82%
$R = \sigma(t\bar{t}H)\times$ BR(H$\to b\bar{b}$)/$\sigma(t\bar{t}Z)\times$BR(Z$\to b\bar{b}$)	$\delta R/R$	1.05%	1.9%
BR(H$\to$ invisible)	BR@95%CL	1×10^{-4}	2.5×10^{-4}

Table 4: Target precision for the parameters relative to the measurement of various Higgs decays, ratios thereof, and of the Higgs self-coupling λ. Notice that Lagrangian couplings have a precision that is typically half that of what is shown here, since all rates and branching ratios depend quadratically on the couplings.

3 Measurement of the Higgs self-coupling

The next experimental goal after the HL-LHC should be to accurately probe the quantum structure of the Higgs potential. A precise measurement of the Higgs self-coupling probes the shape of the Higgs potential near our vacuum and could provide insights about the electro-weak phase transition (EWPT). Although there is no single target that one can propose for this purpose, electroweak loop corrections are typically in the realm of $\mathcal{O}$(few%), thus to begin probing the quantum structure of the Higgs potential the experimental measurement of the Higgs self-coupling need to be sensitive to typical quantum corrections of this magnitude.

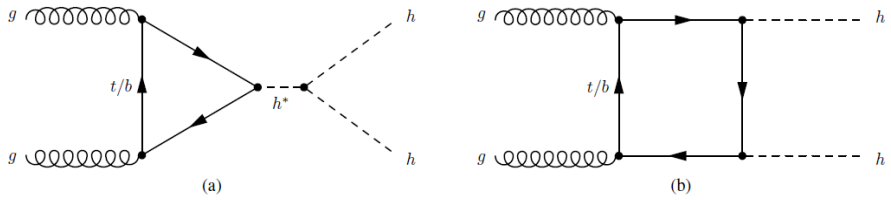

Figure 11: Leading order Feynman diagrams for non-resonant production of Higgs boson pairs in the Standard Model through (a) the Higgs boson self-coupling and (b) the top-box diagram.

At hadron colliders, the Higgs self-coupling can be probed directly via Higgs-pair production. The most studied channel, in view of its large rate, is gluon fusion. In the SM, a large destructive interference between the diagram with the top-quark loop and that with the self-coupling occurs (see Figure 11). While this interference suppresses the SM rate, it makes the rate more sensitive to possible deviations from the SM couplings, the sensitivity being enhanced after NLO corrections are included, as shown in Figure 12. For values of κ_λ close to 1, $1/\sigma_{\mathrm{HH}} d\sigma_{\mathrm{HH}}/d\kappa_\lambda \sim -1$, and a measurement of κ_λ at the few percent level requires therefore the measurement and theoretical interpretation of the Higgs-pair rate at a similar level of precision.

It should be noted that the s-channel "triangle" contribution is suppressed (and the box diagram dominates) at large values of m_{HH}. Conversely the triangle diagram contribution, that contains information on the Higgs self-coupling, is enhanced at low m_{HH}. Information on the Higgs self-coupling can thus be extracted from the differential m_{HH}distribution, provided that the Higgs decay products can be fully reconstructed.

The Higgs self-coupling can be probed via a number of different Higgs boson decay channels. Given the small cross-section, typically at least one of the Higgs bosons is required to decay to a pair of b-quarks. Here, we consider four channels: HH $\to$ b$\bar{\mathrm{b}}\gamma\gamma$, HH $\to$ b$\bar{\mathrm{b}}$ZZ (4ℓ), HH $\to$ b$\bar{\mathrm{b}}$b$\bar{\mathrm{b}}$ + jet and HH $\to$ b$\bar{\mathrm{b}}$WW.

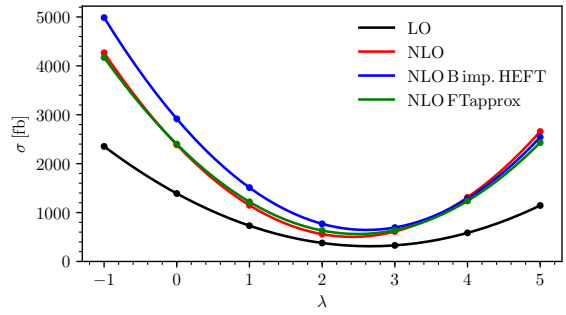

Figure 12: Left: Total gg$\to$HH cross-section at $\sqrt{s} = 100$ TeV as a function of the self-coupling modifier κ_λ for several fixed order calculations [48].

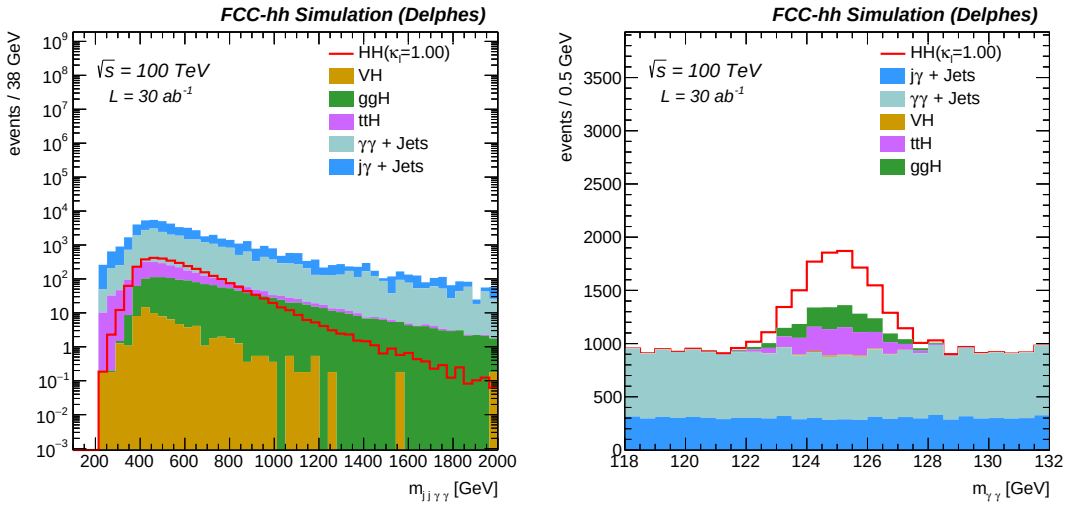

Figure 13: Di-Higgs (left) and di-photon (right) candidates invariant mass spectra after applying all selection criteria.

3.1 $HH \to b\bar{b}\gamma\gamma$

Signal and background events The $b\bar{b}\gamma\gamma$ decay mode provides a very clear signature of two photons and two b-jets in the final state. The main backgrounds are $\gamma\gamma$+jets, γ+jets (with at least one jet being mis-identified as a photon) as well as single Higgs production. The ttH sample has been generated at LO with up to one extra jet merged with the parton shower. The latest NLO cross section $\sigma_{\text{ttH}} = 34$ pb was used for this sample [20]. The gluon fusion single Higgs contribution has been generated at LO in the infinite top mass approximation with an extra $b\bar{b}$ pair. The VH sample has been produced at LO with up to two extra jet merged. The VBF contribution was found to be negligible. The QCD backgrounds $\gamma\gamma$+jets, and γ+ jets have simply been generated at LO. All samples have been generated using the 5 flavour scheme (5F) with a vanishing b-quark mass.

Detector and performance assumptions The photon identification efficiency is assumed to be $\varepsilon_\gamma = 95\%$ for $|\eta| < 2.5$ and $\varepsilon_\gamma = 90\%$ for $2.5 < |\eta| < 4.0$ regardless of the photon p_T. The light jet to photon mis-identification probability (fake-rate) is parameterised by the function $\varepsilon_{j\to\gamma} = 0.002\exp(-p_T[\text{GeV}]/30)$. We assume a nominal resolution on the di-photon pair invariant mass $\delta m_{\gamma\gamma} = 1.3$ GeV. The b-tagging efficiency ε_b and the light (charm) mistag rates $\varepsilon_{l(c)\to b}$ are assumed to be $\varepsilon_b = 85\%$ and $\varepsilon_{l(c)\to b} = 1$ (5)%.

Event selection and signal extraction Events are required to contain at least two isolated photons and two b-tagged jets. Jets are clustered using particle-flow candidates with the anti-k_T algorithm with radius parameter R=0.4. We required $p_{\text{T}}(\gamma,\text{b}) > 30$ GeV and $|\eta(\gamma,\text{b})| < 3.0$. The Higgs candidates are formed from the two jets and photons with highest $p_{\text{T}}(\gamma,\text{b})$. The leading photon and b-jet are required to have $p_{\text{T}}(\gamma,\text{b}) > 60$ GeV, and the di-photon and di-jet pairs $p_{\text{T}}(\gamma\gamma,\text{b}\bar{\text{b}}) > 125$ GeV. In order to suppress the ttH background, we veto leptons with $p_{\text{T}}(\ell) > 25$ GeV and $|\eta(\ell)| < 3.0$ and require $\Delta R_{\text{b}\bar{\text{b}}} < 2.0$. Finally, we apply a window cut on the invariant mass of the $b\bar{b}$pair $100 < m_{\text{bb}} < 130$ GeV. The signal extraction is performed via a 2-dimensional likelihood fit over the the photon pair and the Higgs pair invariant masses, $m_{\gamma\gamma}$ and m_{HH}, shown in Figure 13 (left) and (right). The signal shape is parameterized by a Gaussian and the sum of a Landau and an exponential distribution respectively.

Results and discussion The negative log-likelihood (NLL) distribution for the parameter κ_λ with respect to the best-fit value obtained for varying systematics, background normalisation and detector

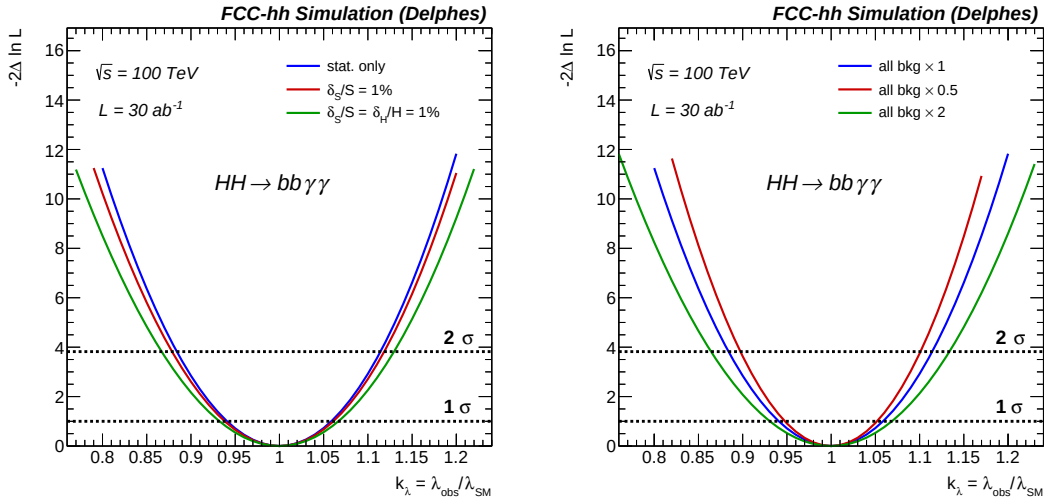

Figure 14: Expected precision on the Higgs self-coupling modifier κ_λ with no systematic uncertainties (only statistical), 1% signal uncertainty, 1% signal uncertainty together with 1% uncertainty on the Higgs backgrounds (left) and assuming respectively $\times 1$, $\times 2$, $\times 0.5$ background yields (right).)

assumptions is shown in Figures 14 and 15. The 1σ and 2σ lines correspond to the 68% and 95% confidence levels (CL) respectively.

Figure 14 (left) shows the sensitivity obtained with different assumptions about the uncertainties. With only the statistical uncertainty (blue curve), we find $\delta\kappa_\lambda = 5.5\%$. When a 1% systematic uncertainty on the signal normalisation is included (red curve) the expected precision decreases to $\delta\kappa_\lambda = 6\%$. An additional uncertainty of 1% on the single Higgs backgrounds normalisation (green curve) is shown under the assumption that the QCD background can be extrapolated from a control sample with high statistics defined by $|m_{\gamma\gamma} - m_{\mathrm{H}}| > 10$ GeV into the signal region. For the single Higgs background defining such a control sample is more challenging and we therefore assume an uncertainty of 1% on the normalisation, motivated by expected precision on single Higgs rates at the FCC-hh [43]. In this scenario we find an expected precision $\delta\kappa_\lambda = 6.5\%$. Figure 14 (right) shows how the precision is affected by varying the overall background yields by factors of 2 and 0.5 and find an impact on the overall κ_λ precision of $\approx \pm 1\%$.

Figure 15 shows the impact of detector performance related assumptions on the sensitivity. Figure 15 (left) shows the impact of degrading the energy resolution of the electromagnetic calorimeter, which affects the $\Delta m_{\gamma\gamma}$ resolution. Figure 15 (center) shows the impact of varying the photon reconstruction efficiency and Figure 15 (right) shows the impact of varying the jet-to-photon fake rate. Each of these scenarios degrades the precision on the self-coupling by 1-2%, highlighting the importance of designing a detector with excellent photon energy resolution and fake rejection capabilities. These less optimistic performance assumptions roughly correspond to the expected performance of the ATLAS and CMS detectors at High-Luminosity LHC [49, 50].

To summarize, within the stated assumptions on the expected performance of the FCC-hh detector, a statistical precision on the Higgs self-coupling of $\delta\kappa_\lambda = 5\%$ in the HH $\to$ bb$\gamma\gamma$ channel can be achieved.

3.2 HH $\to$ b$\bar{\mathrm{b}}$ZZ (4ℓ)

The large Higgs pair production cross section at 100 TeV allows for rare but cleaner final states to become accessible. One example is the HH $\to$ b$\bar{\mathrm{b}}$ZZ (4ℓ) decay channel (where $\ell = \mathrm{e}^{\pm}, \mu^{\pm}$). Despite a small cross section ($\sigma_{\mathrm{HH}\to \mathrm{b\bar{b}ZZ}\ (4\ell)} = 178$ ab), the presence of four leptons in association with two b-jets leads

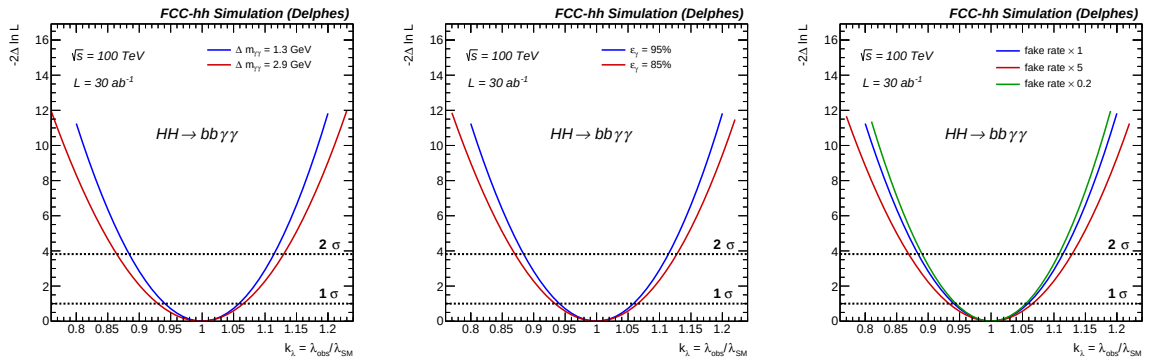

Figure 15: Expected precision on the Higgs self-coupling modifier κ_λ obtained by varying the photon reconstruction performance. Left: Comparison of two scenarios with nominal ($\Delta m_{\gamma\gamma} = 1.3$ GeV) and degraded ($\Delta m_{\gamma\gamma} = 2.9$ GeV) energy resolution. Center: Comparison of two scenarios with nominal ($\varepsilon_\gamma = 95\%$) and degraded ($\varepsilon_\gamma = 85\%$) photon reconstruction efficiency. Right: Comparison of three scenarios with nominal (see eq.), degraded ($\times 5$) and improved ($\times 0.2$) photon mistag rate.

to a very clean final state topology allowing to maintain a rather good signal selection efficiency while keeping the background contribution small. The main backgrounds processes are ttH (4ℓ), H(4ℓ)+b$\bar{\text{b}}$, Z(b$\bar{\text{b}}$)H(4ℓ), and t$\bar{\text{t}}Z$ (2ℓ), followed by minor negligible contributions such as 4ℓ+b$\bar{\text{b}}$ continuum, t$\bar{\text{t}}$H($\mu\mu$) and t$\bar{\text{t}}$ZZ(4ℓ).

The ttH, H+b$\bar{\text{b}}$, ZH, and t$\bar{\text{t}}Z$ (2ℓ) background samples were generated at LO and higher order radiative corrections were accounted for by applying K-factors of $K(\text{ttH}) = 1.22$, $K(\text{ggH}) = 3.2$ and $K(\text{ZH}) = 1.1$ (extracted from [20]). The contribution of the 4ℓ+jets continuum is evaluated using a $\ell\ell\ell\ell$jj sample, generated with the four leptons invariant mass in the range [100, 150] GeV and only heavy flavour partons (b/c). This background contribution was found to be negligible.

Event Selection Events are required to have exactly four identified and isolated muons (electrons) with $p_{\text{T}} > 5(7)$ GeV and $|\eta| < 4.0$. Z boson candidates are formed from pairs of opposite-charge leptons ($\ell^+\ell^-$). At least two di-lepton pairs are required. The Z candidate with the invariant mass closest to the nominal Z mass is denoted as Z_1; then, among the other opposite-sign lepton pairs, the one with the highest p_T is labelled as Z_2. Z candidates must pass a set of kinematic requirements: the Z_1 and Z_2 invariant masses have to be in the [40, 120] GeV and [12, 120] GeV ranges, respectively. At least one lepton is required to have $p_{\text{T}} > 20$ GeV and a second is required to have $p_{\text{T}} > 10$ GeV. A minimum angular separation $\Delta R(\ell_i, \ell_j) > 0.02$ between two leptons is required. The four leptons invariant mass, $m_{4\ell}$, is requested to be in the range $120 < m_{4\ell} < 130$ GeV.

At least two identified b-jets, reconstructed with the anti-k_T algorithm inside a cone of radius $R = 0.4$, are required. Their invariant mass is required to be in the range $80 < m_{\text{b}\bar{\text{b}}} < 130$ GeV and the angular distance between the 2 b-jets has to be $0.5 < \Delta R_{\text{b}\bar{\text{b}}} < 2$. These cuts are particularly effective to reject the ttH background.

Results The invariant mass spectrum of the four leptons after the full event selection is shown in Figure 16 (left). The negative log-likelihood on the self-coupling modifier κ_λ is shown in Figure 16, (right), for three different systematics assumptions:

1. Statistical uncertainties only
2. 1% systematic uncertainty on signal and background: $\frac{\Delta S}{S} = \frac{\Delta B}{B} = 1\%$

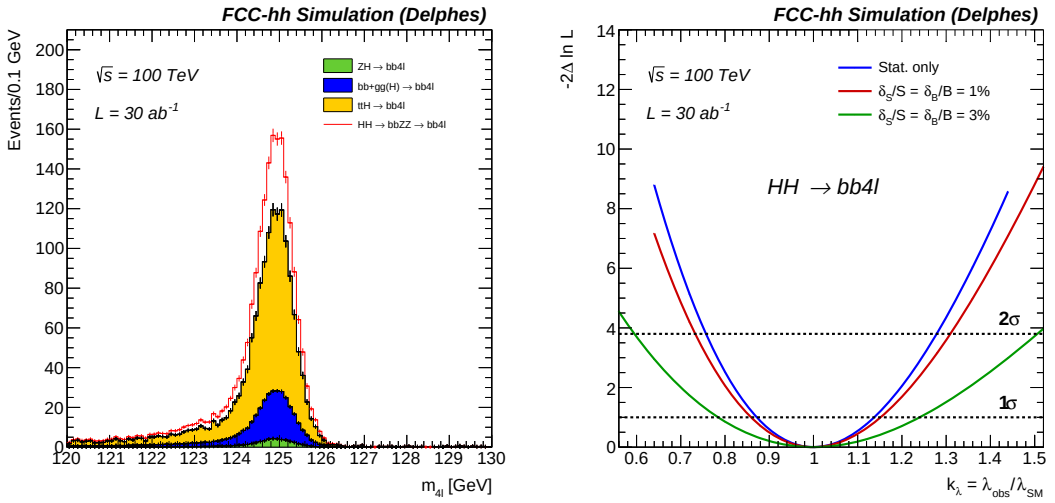

Figure 16: Left: Stacked plot of the four leptons invariant mass for the HH $\rightarrow$ b$\bar{\text{b}}$ZZ (4ℓ) signal and all the analysed background processes after the full selection for 30 ab^{-1}. Right: Expected precision on the Higgs-self coupling.

3. 3% systematic uncertainty on signal and background: $\frac{\Delta S}{S} = \frac{\Delta B}{B} = 3\%$

The expected precision on the Higgs self-coupling modifier κ_λ without systematics is 14% at 68% CL. When assuming a 1% systematic uncertainty on the signal and the backgrounds the precision on κ_λ becomes 15% and with a 3% systematic uncertainty it decreases to 24%.

3.3 HH $\rightarrow$ b$\bar{\text{b}}$b$\bar{\text{b}}$ + jet

The channel HH$\rightarrow$b$\bar{\text{b}}$b$\bar{\text{b}}$ is interesting to investigate due to the large Higgs branching fraction to a b$\bar{\text{b}}$ pair. The overwhelming QCD background can be reduced by requiring the Higgs to be boosted such that the decay products are contained inside a single, large radius jet. A boosted configuration in which the two Higgs bosons have a large boost and recoil against each other can be effective in terms of background rejection but without further requirements this configuration provides low sensitivity to the Higgs self-coupling since the di-Higgs rate dependence on the tri-linear largely originates from configurations with low m_{HH}. Following the approach in [51], we study the configuration where the Higgs pair recoils against one or more jets, forcing the pair to have a small invariant mass. The main backgrounds include at least four b-jets, where the two b$\bar{\text{b}}$ pairs come from either strong production (QCD), mainly from $g \rightarrow$ b$\bar{\text{b}}$ splittings, either QCD and electroweak production (QCD+EWK), e.g. Zb$\bar{\text{b}}$, or pure EW production, e.g. ZH or ZZ.

The signal sample consists in HH+jet and was generated taking into account the full top mass dependence at leading order (LO) with the jet $p_{\text{T}}^{\text{jet}}$ (or equivalently the di-Higgs p_{T}^{HH}), $p_{\text{T}} > 200$ GeV, accounting for the full top mass. Higher order QCD corrections are accounted for with a K-factor K =1.95 applied to the signal samples [51], leading to $\sigma_{\text{HHj}} = 38$ fb for $p_{\text{T}}^{\text{jet}} > 200$ GeV and κ_λ=1. The LO background cross-sections are computed with $p_{\text{T}}^{\text{jet}} > 200$ GeV and are $\sigma_{\text{b}\bar{\text{b}}\text{b}\bar{\text{b}}}(\text{QCD}) = 443.1$ pb, $\sigma_{\text{b}\bar{\text{b}}\text{b}\bar{\text{b}}\text{j}}(\text{QCD+EWK}) = 6.2$ pb and $\sigma_{\text{b}\bar{\text{b}}\text{b}\bar{\text{b}}\text{j}}(\text{EWK}) = 72$ fb.

Event selection and signal extraction Jets are clustered using particle-flow candidates with the anti-k_{T} algorithm with a large parameter R=0.8. The large cone size is chosen such that a large fraction of the Higgs decay products will be included in the jet, hence the denomination "fat-jets". Events are first pre-selected by requiring at least two central fat jets that contain at least two b-subjets. We assume

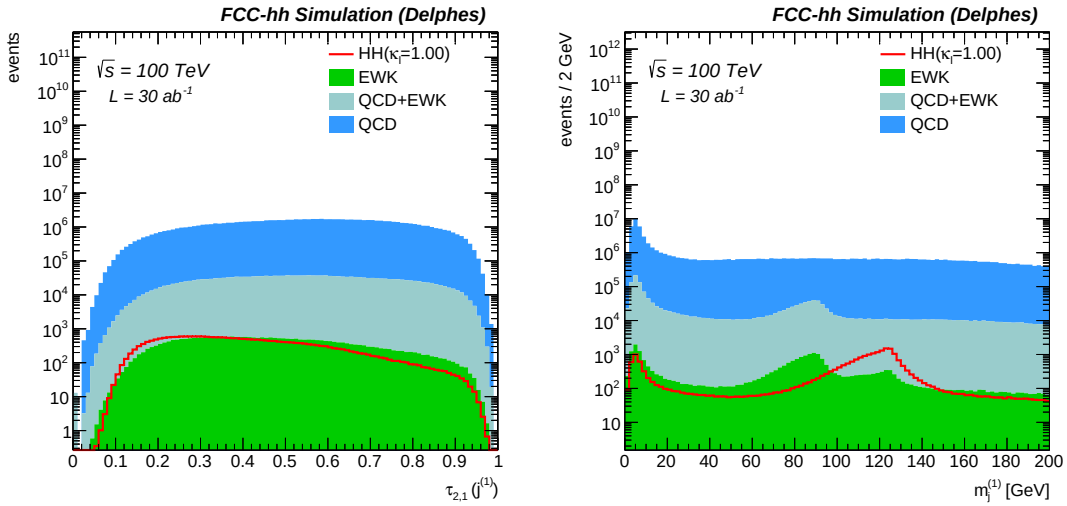

Figure 17: 2-to-1 ($\tau_{2,1}$) subjettiness ratio (left) and softDropped mass (left) spectra of the leading Higgs fat-jet candidate.

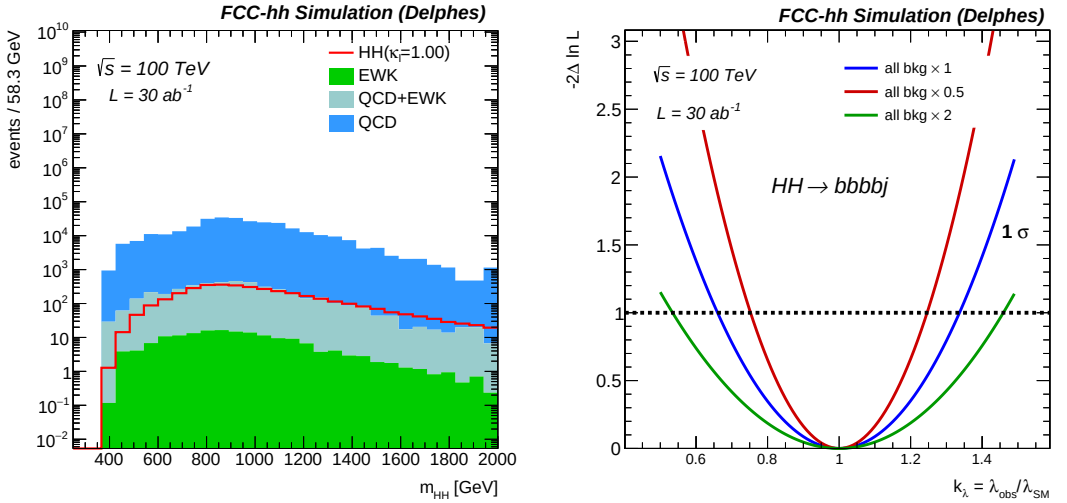

Figure 18: Left: Invariant mass spectrum of the di-Higgs pair constructed from the two fat-jet higgs candidates after the full event selection. Right: Expected precision on the Higgs self-coupling modifier κ_λ assuming respectively $\times 1$, $\times 2$, $\times 0.5$ the nominal background yields.)

a conservative 70% b-tagging efficiency. The fat-jets are selected if $p_T^j > 300$ GeV and $|p_T^j| < 2.5$. The two highest momentum double b-tagged fat-jets constitute our Higgs candidates. We further ask the di-fatjet pair to be sufficiently boosted, $p_T^{jj} > 250$ GeV, and the leading jet to have a $p_T^j > 400$ GeV. The N-subjettiness ratio $\tau_{2,1}$ observable [46] is shown in Figure 17 (left) and the soft-dropped mass m_{SD} is shown in Figure 17 (right). Higgs jets are tagged by selecting jets with $\tau_{2,1} < 0.35$ and $100 < m_{SD} < 130$ GeV, which yields a signal tagging efficiency of 6% and a background mis-identification rate of 0.1%. Each of the two fat jets is required to be tagged. The signal extraction is performed via a one-dimensional likelihood fit on the di-Higgs mass observable m_{HH}, shown in Figure 18 (left).

Results and discussion The negative log-likelihood (NLL) distribution of the parameter κ_λ is shown in Figure 18 (right). For the nominal detector and background yield assumptions we find an

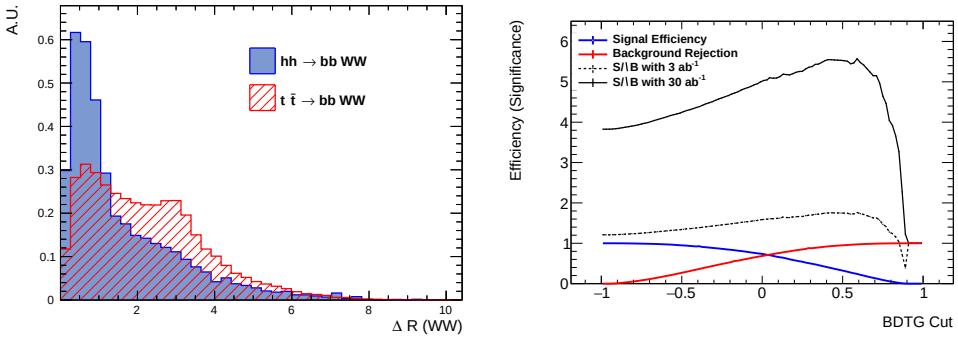

Figure 19: Left: The distribution of the most discriminant variables used in the BDT training for discriminating signal and background samples: the ΔR between the two W's. Right: The BDT efficiency and significance as a function of the applied cut on the BDT response for two reference integrated luminosity values: 3 ab^{-1} and 30 ab^{-1}.

expected precision of the self-coupling of $\delta\kappa_\lambda = 30\%$. The uncertainty on the QCD background yield is parametrised by varying the overall normalisation by factors of 2 and 0.5 yielding an impact of the overall κ_λ precision by $\approx \pm 10\%$.

This measurement can be improved by extending the analysis in the semi-resolved phase space region, where one Higgs is boosted and forms a fat-jet and the other is resolved, and into the fully resolved region with 4 b-jets in the final state.

3.4 HH $\rightarrow$ b$\bar{\text{b}}$WW

For the bbWW decay mode, only the channel where one W boson to decay hadronically and the other leptonically is considered. The dominant backgrounds are t$\bar{\text{t}}$ and multi-jet background, with smaller contributions from Drell-Yan and single top-quark production. Events are required to meet the following requirements: $p_{\text{T}}(\text{WW}) > 150$ GeV, an invariant mass of the two b-jets system of $80 < m_{\text{bb}} < 180$ GeV and an angular distance between the two b-jets system of $\Delta R_{\text{bb}} < 2.0$.

The signal selection is optimized using a boosted decision tree (BDT). The input variables used by the BDT are the leptons, the jets and the neutrino 4-momenta as well as the azimutal angular distance between various objects. The BDT is trained to discriminate the signal from the dominant background t$\bar{\text{t}}$. The event selection on the BDT output score has been optimised to ensure a high significance ratio (where S is the number of signal events and B the number of background events after the full event selection).

An example of an input distribution used in the BDT is shown in Figure 19 (a), which is the angular separation between the two W bosons. The output BDT distribution for the signal and background is shown in Figure 19 (b). With $\mathscr{L} = 30$ ab^{-1}, a significance of 5σ can be achieved using the bbWW decay mode, corresponding to a precision of $\delta\kappa_\lambda = 40\%$

3.5 Summary of Higgs self-coupling studies

A summary of the target precision in the measurement of κ_λ is given in Table 5. Reference [51] proposed using a boosted HH final state to enhance the self-coupling sensitivity in the case of the b$\bar{\text{b}}\tau\tau$ final state, following the approach discussed in Section3.3. A precision $\delta\kappa_\lambda \pm 8\%$ can obtained at 68%CL in this decay mode and we include in the summary table for completeness. Within the stated assumptions on the expected performance of the FCC-hh detector, a precision target on the Higgs self-coupling of

$\delta\kappa_\lambda = 5\%$ appears achievable, by exploiting several techniques and decay modes, and assuming the future theoretical progress in modelling signals and backgrounds.

	$b\bar{b}\gamma\gamma$	$b\bar{b}\tau\tau$	$b\bar{b}ZZ^*[\to 4\ell]$	$b\bar{b}WW^*[\to 2j\ell\nu]$	4b+jet
$\delta\kappa_\lambda$	6%	8%	14%	40%	30%

Table 5: Precision of the direct Higgs self-coupling measurement in gg→HH production at $\sqrt{s} = 100$ TeV with $\mathscr{L} = 30$ ab^{-1} for various decay modes.

References

[1] G. Aad et al., ATLAS, *Observation of a new particle in the search for the Standard Model Higgs boson with the ATLAS detector at the LHC*, Phys. Lett. **B716** (2012) 1, DOI: 10.1016/j.physletb.2012.08.020, arXiv: 1207.7214 [hep-ex].

[2] S. Chatrchyan et al., CMS, *Observation of a new boson at a mass of 125 GeV with the CMS experiment at the LHC*, Phys. Lett. **B716** (2012) 30, DOI: 10.1016/j.physletb.2012.08.021, arXiv: 1207.7235 [hep-ex].

[3] F. Englert, R. Brout, *Broken Symmetry and the Mass of Gauge Vector Mesons*, Phys. Rev. Lett. **13** (1964), [,157(1964)] 321, DOI: 10.1103/PhysRevLett.13.321.

[4] P. W. Higgs, *Broken symmetries, massless particles and gauge fields*, Phys. Lett. **12** (1964) 132, DOI: 10.1016/0031-9163(64)91136-9.

[5] P. W. Higgs, *Broken Symmetries and the Masses of Gauge Bosons*, Phys. Rev. Lett. **13** (1964), [,160(1964)] 508, DOI: 10.1103/PhysRevLett.13.508.

[6] G. S. Guralnik, C. R. Hagen, T. W. B. Kibble, *Global Conservation Laws and Massless Particles*, Phys. Rev. Lett. **13** (1964), [,162(1964)] 585, DOI: 10.1103/PhysRevLett.13.585.

[7] P. W. Higgs, *Spontaneous Symmetry Breakdown without Massless Bosons*, Phys. Rev. **145** (1966) 1156, DOI: 10.1103/PhysRev.145.1156.

[8] T. W. B. Kibble, *Symmetry breaking in nonAbelian gauge theories*, Phys. Rev. **155** (1967), [,165(1967)] 1554, DOI: 10.1103/PhysRev.155.1554.

[9] V. F. Weisskopf, *On the Self-Energy and the Electromagnetic Field of the Electron*, Phys. Rev. **56** (1939) 72, DOI: 10.1103/PhysRev.56.72.

[10] M. Cepeda et al., Physics of the HL-LHC Working Group, *Higgs Physics at the HL-LHC and HE-LHC* (2019), arXiv: 1902.00134 [hep-ph].

[11] M. Mangano et al., *Future Circular Collider* (2018).

[12] J. Alwall et al., *MadGraph 5 : Going Beyond*, JHEP **06** (2011) 128, DOI: 10.1007/JHEP06(2011)128, arXiv: 1106.0522 [hep-ph].

[13] T. Sjöstrand et al., *An Introduction to PYTHIA 8.2*, Comput. Phys. Commun. **191** (2015) 159, DOI: 10.1016/j.cpc.2015.01.024, arXiv: 1410.3012 [hep-ph].

[14] J. de Favereau et al., DELPHES 3, *DELPHES 3, A modular framework for fast simulation of a generic collider experiment*, JHEP **02** (2014) 057, DOI: 10.1007/JHEP02(2014)057, arXiv: 1307.6346 [hep-ex].

[15] M. Benedikt et al., *Future Circular Collider Study. Volume 3: The Hadron Collider (FCC-hh)*, tech. rep. CERN-ACC-2018-0058, Submitted for publication to Eur. Phys. J. ST., Geneva: CERN, 2018, URL: https://cds.cern.ch/record/2651300.

[16] *FCC-hh detector DELPHES card*, https://github.com/delphes/delphes/blob/master/cards/FCC/FCChh.tcl.

[17] A. M. Sirunyan et al., CMS, *Combination of searches for Higgs boson pair production in proton-proton collisions at $\sqrt{s} = 13$ TeV*, Submitted to: Phys. Rev. Lett. (2018), arXiv: 1811.09689 [hep-ex].

[18] ATLAS Collaboration, *Combined measurements of Higgs boson production and decay using up to 80 fb^{-1} of proton–proton collision data at $\sqrt{s} = 13$ TeV collected with the ATLAS experiment*, tech. rep. ATLAS-CONF-2018-031, Geneva: CERN, 2018, URL: https://cds.cern.ch/record/2629412.

[19] M. Benedikt et al., *Future Circular Collider Study. Volume 2: The Lepton Collider (FCC-ee)*, tech. rep. CERN-ACC-2018-0057, Submitted for publication to Eur. Phys. J. ST., Geneva: CERN, 2018, URL: https://cds.cern.ch/record/2651299.

[20] R. Contino et al., *Physics at a 100 TeV pp collider: Higgs and EW symmetry breaking studies*, CERN Yellow Report (2017) 255, DOI: 10.23731/CYRM-2017-003.255, arXiv: 1606.09408 [hep-ph].

[21] M. L. Mangano et al., *ALPGEN, a generator for hard multiparton processes in hadronic collisions*, JHEP **07** (2003) 001, DOI: 10.1088/1126-6708/2003/07/001, arXiv: hep-ph/0206293 [hep-ph].

[22] B. Mellado Garcia et al., *CERN Report 4: Part I Standard Model Predictions* (2016), URL: https://cds.cern.ch/record/2150771.

[23] M. L. Mangano et al., *Physics at a 100 TeV pp Collider: Standard Model Processes*, CERN Yellow Report (2017) 1, DOI: 10.23731/CYRM-2017-003.1, arXiv: 1607.01831 [hep-ph].

[24] A. M. Sirunyan et al., CMS, *Particle-flow reconstruction and global event description with the CMS detector*, JINST **12** (2017) P10003, DOI: 10.1088/1748-0221/12/10/P10003, arXiv: 1706.04965 [physics.ins-det].

[25] C. Anastasiou et al., *Higgs Boson Gluon-Fusion Production in QCD at Three Loops*, Phys. Rev. Lett. **114** (2015) 212001, DOI: 10.1103/PhysRevLett.114.212001, arXiv: 1503.06056 [hep-ph].

[26] A. M. Sirunyan et al., CMS, *Measurements of Higgs boson properties in the diphoton decay channel in proton-proton collisions at $\sqrt{s} = 13$ TeV* (2018), arXiv: 1804.02716 [hep-ex].

[27] R. E. Shrock, M. Suzuki, *Invisible decays of Higgs bosons*, Physics Letters B **110** (1982) 250, ISSN: 0370-2693, DOI: https://doi.org/10.1016/0370-2693(82)91247-3, URL: http://www.sciencedirect.com/science/article/pii/0370269382912473.

[28] A. Djouadi et al., *Implications of LHC searches for Higgs-portal dark matter*, Physics Letters B **709** (2012) 65, ISSN: 0370-2693, DOI: https://doi.org/10.1016/j.physletb.2012.01.062, URL: http://www.sciencedirect.com/science/article/pii/S0370269312001037.

[29] S. Baek et al., *Higgs portal vector dark matter: revisited*,
Journal of High Energy Physics **2013** (2013) 36, ISSN: 1029-8479,
DOI: 10.1007/JHEP05(2013)036,
URL: https://doi.org/10.1007/JHEP05(2013)036.

[30] A. Djouadi et al., *Direct detection of Higgs–portal dark matter at the LHC*,
The European Physical Journal C **73** (2013) 2455, ISSN: 1434-6052,
DOI: 10.1140/epjc/s10052-013-2455-1,
URL: https://doi.org/10.1140/epjc/s10052-013-2455-1.

[31] A. Beniwal et al., *Combined analysis of effective Higgs portal dark matter models*,
Phys. Rev. D **93** (11 2016) 115016, DOI: 10.1103/PhysRevD.93.115016,
URL: https://link.aps.org/doi/10.1103/PhysRevD.93.115016.

[32] A. M. Sirunyan et al., CMS, *Search for new physics in final states with an energetic jet or a hadronically decaying W or Z boson and transverse momentum imbalance at* $\sqrt{s} = 13$ TeV,
Phys. Rev. **D97** (2018) 092005, DOI: 10.1103/PhysRevD.97.092005,
arXiv: 1712.02345 [hep-ex].

[33] M. Aaboud et al., ATLAS, *Search for dark matter and other new phenomena in events with an energetic jet and large missing transverse momentum using the ATLAS detector*,
JHEP **01** (2018) 126, DOI: 10.1007/JHEP01(2018)126,
arXiv: 1711.03301 [hep-ex].

[34] J. M. Lindert et al., *Precise predictions for V+ jets dark matter backgrounds*,
Eur. Phys. J. **C77** (2017) 829, DOI: 10.1140/epjc/s10052-017-5389-1,
arXiv: 1705.04664 [hep-ph].

[35] R. Frederix, S. Frixione, *Merging meets matching in MC@NLO*, JHEP **12** (2012) 061,
DOI: 10.1007/JHEP12(2012)061, arXiv: 1209.6215 [hep-ph].

[36] A. Djouadi et al., *Direct Detection of Higgs-Portal Dark Matter at the LHC*,
Eur. Phys. J. **C73** (2013) 2455, DOI: 10.1140/epjc/s10052-013-2455-1,
arXiv: 1205.3169 [hep-ph].

[37] D. S. Akerib et al., LUX, *Results from a search for dark matter in the complete LUX exposure*,
Phys. Rev. Lett. **118** (2017) 021303, DOI: 10.1103/PhysRevLett.118.021303,
arXiv: 1608.07648 [astro-ph.CO].

[38] A. Tan et al., PandaX-II,
Dark Matter Results from First 98.7 Days of Data from the PandaX-II Experiment,
Phys. Rev. Lett. **117** (2016) 121303, DOI: 10.1103/PhysRevLett.117.121303,
arXiv: 1607.07400 [hep-ex].

[39] R. Agnese et al., SuperCDMS, *New Results from the Search for Low-Mass Weakly Interacting Massive Particles with the CDMS Low Ionization Threshold Experiment*,
Phys. Rev. Lett. **116** (2016) 071301, DOI: 10.1103/PhysRevLett.116.071301,
arXiv: 1509.02448 [astro-ph.CO].

[40] J. Billard, L. Strigari, E. Figueroa-Feliciano, *Implication of neutrino backgrounds on the reach of next generation dark matter direct detection experiments*, Phys. Rev. **D89** (2014) 023524,
DOI: 10.1103/PhysRevD.89.023524, arXiv: 1307.5458 [hep-ph].

[41] A. M. Sirunyan et al., CMS, *Observation of* $\mathrm{t\bar{t}}H$ *production*, Phys. Rev. Lett. **120** (2018) 231801,
DOI: 10.1103/PhysRevLett.120.231801, arXiv: 1804.02610 [hep-ex].

[42] M. Aaboud et al., ATLAS, *Observation of Higgs boson production in association with a top quark pair at the LHC with the ATLAS detector* (2018), arXiv: 1806.00425 [hep-ex].

[43] M. L. Mangano et al., *Measuring the Top Yukawa Coupling at 100 TeV*, J. Phys. **G43** (2016) 035001, DOI: 10.1088/0954-3899/43/3/035001, arXiv: 1507.08169 [hep-ph].

[44] M. Cacciari, G. P. Salam, G. Soyez, *The anti-k_t jet clustering algorithm*, JHEP **04** (2008) 063, DOI: 10.1088/1126-6708/2008/04/063, arXiv: 0802.1189 [hep-ex].

[45] A. J. Larkoski et al., *Soft Drop*, JHEP **05** (2014) 146, DOI: 10.1007/JHEP05(2014)146, arXiv: 1402.2657 [hep-ph].

[46] J. Thaler, K. Van Tilburg, *Identifying Boosted Objects with N-subjettiness*, JHEP **03** (2011) 015, DOI: 10.1007/JHEP03(2011)015, arXiv: 1011.2268 [hep-ph].

[47] R. A. Gerosa, CMS Collaboration, *Vector Boson Scattering prospects for High-Luminosity LHC at CMS in the same sign WW final state*, tech. rep. CMS-CR-2015-219, Geneva: CERN, 2015, URL: http://cds.cern.ch/record/2058229.

[48] S. Borowka et al., *Full top quark mass dependence in Higgs boson pair production at NLO*, JHEP **10** (2016) 107, DOI: 10.1007/JHEP10(2016)107, arXiv: 1608.04798 [hep-ph].

[49] D. Contardo et al., *Technical Proposal for the Phase-II Upgrade of the CMS Detector* (2015).

[50] ATLAS Collaboration, *Expected performance for an upgraded ATLAS detector at High-Luminosity LHC*, tech. rep. ATL-PHYS-PUB-2016-026, Geneva: CERN, 2016, URL: https://cds.cern.ch/record/2223839.

[51] S. Banerjee et al., *$hh+$jet production at 100 TeV*, Eur. Phys. J. **C78** (2018) 322, DOI: 10.1140/epjc/s10052-018-5788-y, arXiv: 1802.01607 [hep-ph].